



# Exosomal miR-375-3p breaks vascular barrier and promotes small cell lung cancer metastasis by targeting claudin-1

Shuangshuang Mao<sup>1</sup>, Sufei Zheng<sup>1</sup>, Zhiliang Lu<sup>1</sup>, Xinfeng Wang<sup>1</sup>, Yan Wang<sup>2</sup>, Guochao Zhang<sup>1</sup>, Haiyan Xu<sup>3</sup>, Jianbing Huang<sup>1</sup>, Yuanyuan Lei<sup>1</sup>, Chengming Liu<sup>1</sup>, Nan Sun<sup>1</sup>, Jie He<sup>1</sup>

<sup>1</sup>Department of Thoracic Surgery, National Cancer Center/National Clinical Research Center for Cancer/Cancer Hospital, Chinese Academy of Medical Sciences and Peking Union Medical College, Beijing, China; <sup>2</sup>Department of Medical Oncology, National Cancer Center/National Clinical Research Center for Cancer/Cancer Hospital, Chinese Academy of Medical Sciences and Peking Union Medical College, Beijing, China; <sup>3</sup>Department of Comprehensive Oncology, National Cancer Center/National Clinical Research Center for Cancer/Cancer Hospital, Chinese Academy of Medical Sciences and Peking Union Medical College, Beijing, China

**Contributions:** (I) Conception and design: J He, N Sun; (II) Administrative support: J He, N Sun; (III) Provision of study materials or patients: S Mao, S Zheng, Z Lu, X Wang, Y Wang, H Xu, G Zhang; (IV) Collection and assembly of data: S Mao, S Zheng, Z Lu, X Wang; (V) Data analysis and interpretation: S Mao, S Zheng, Z Lu, J Huang, Y Lei, C Liu; (VI) Manuscript writing: All authors; (VII) Final approval of manuscript: All authors.

**Correspondence to:** Jie He; Nan Sun. Department of Thoracic Surgery, National Cancer Center/National Clinical Research Center for Cancer/Cancer Hospital, Chinese Academy of Medical Sciences and Peking Union Medical College, Beijing 100021, China. Email: prof.jiehe@gmail.com; sunnan@vip.126.com.

**Background:** High incidence of metastasis is the main cause of death for small cell lung cancer (SCLC), with its underlying molecular mechanisms remain unclear. Exosomal miRNAs are important regulators in metastatic processes of various tumors, but their specific role in SCLC metastasis is unknown.

**Methods:** Small RNA sequencing followed by qRT-PCR verification was used to screen the potential exosomal miRNAs that might mediate SCLC metastasis. SCLC-cell-secreted exosomes were labeled followed by incubating with vascular endothelial cells to evaluate exosome-mediated communication between SCLC cells and vascular endothelial cells. In vitro permeability assay and transendothelial migration assay were applied to investigate the function of exosomal miRNA on vascular endothelial cells. *In vivo* permeability assay and mouse lung colonization assay were used to verify the effects of exosomal miRNA on vascular barriers and SCLC metastasis *in vivo*. Proteomics technology, dual-luciferase reporter system together with rescue assays were conducted to excavate the downstream pathways of miRNA.

**Results:** Compared with 57 healthy volunteers and 46 non-small cell lung cancer patients, we identified that the level of exosomal miR-375-3p in 126 SCLC patients was obviously higher and was positively correlated with patient TNM stages. In vitro functional experiments found that SCLC-cell-secreted exosomal miR-375-3p could increase the permeability of vascular endothelial cells and facilitate the transendothelial migration of SCLC cells. *In vivo*, miR-375-3p-enriched exosomes also destroyed the barrier structure of lung, liver and brain tissues of mice, led to an increased blood vessel permeability and finally promoted SCLC metastasis. Mechanistically, SCLC-cell-secreted exosomal miR-375-3p was transferred to vascular endothelial cells. The internalized miR-375-3p broke the tight junction of vascular endothelial cells by directly binding to the 3'UTR of tight junction protein claudin-1 and negatively regulating its expression. Overexpressing claudin-1 in vascular endothelial cells could rescue the broken vascular barriers induced by miR-375-3p.

**Conclusions:** Our findings underline the crucial roles of exosomal miRNA-375-3p in regulating vascular endothelial barrier integrity and SCLC metastasis. miRNA-375-3p has a great potential to be a novel biomarker monitoring metastasis and guiding clinical therapeutics of SCLC patients.

**Keywords:** Exosomes; miR-375-3p; small cell lung cancer (SCLC); metastasis; vascular permeability

Submitted Apr 30, 2021. Accepted for publication Jun 21, 2021.

doi: 10.21037/tlcr-21-356

**View this article at:** <https://dx.doi.org/10.21037/tlcr-21-356>

## Introduction

Small cell lung cancer (SCLC), an extremely malignant and deadly subtype of lung cancer, is different from other lung cancers in terms of pathology, molecular biology and clinical manifestation (1,2). Accounting for nearly 15% of lung cancer cases (3-6), SCLC is the sixth common cause of cancer-related mortality (7) and leads to an estimated 250,000 deaths worldwide every year (1). The malignancy and lethality of SCLC are attributed to its extremely aggressive biological characteristics, especially its high potential for metastasis (1,7,8). Among all patients with SCLC, approximately two-thirds are diagnosed with advanced-stage disease that is generally accompanied by distant metastasis and has a five-year survival rate of <5% (9). Platinum plus etoposide is the first choice for these SCLC patients and this strategy has not changed in three decades (10); unfortunately, most patients experience disease relapse and drug resistance within 6 months (11). Uncovering the underlying molecular mechanisms of SCLC metastasis will be of great value in improving SCLC patient prognosis and is urgently needed in the clinic.

Exosomes were small extracellular vesicles originated from multivesicular endosome pathways and contain various biological molecules, including DNA, mRNA, microRNA (miRNA), proteins and lipids, which mediate intercellular communications between cells and microenvironments (12). Tumor-secreted exosomes have been widely documented to act essential roles in primary tumor growth, distant metastasis, neovascularization and escape from immunosurveillance (13-16), and exosome-based drug delivery also showed great potential in cancer therapeutics (17). miRNAs, one of the major components packaged in exosomes, mediate the destabilization or translation inhibition of mRNA by targeting the 3' untranslated regions (3' UTRs) of mRNAs (18), and upregulation or downregulation of miRNAs is closely correlated with cancer development and evolution (19). miRNAs loaded into exosomes are transferred from secreted cells to exert their post-transcriptional regulation of target genes in recipient cells to construct a comfortable microenvironment supporting tumor survival and evolution (20-22). Recently, the effects of tumor-secreted exosomal miRNAs on vascular endothelial cells and their further promoting roles in cancer metastasis have attracted researchers' attention, and many researches have shown that tumor-secreted exosomal miRNAs can promote metastasis by targeting vascular endothelial cells to induce angiogenesis or increase vascular permeability (23-25). However, how tumor-secreted exosomal miRNAs promote SCLC

metastasis by affecting vascular endothelial cells remain poorly understood.

Herein, we compared the plasma exosomal miRNA omics of SCLC patients with or without metastasis and identified a potential miRNA, miR-375-3p, which was obviously upregulated in plasma exosomes of SCLC patients with tumor metastasis. Recently, the dysregulation of exosomal miR-375 and its important roles in tumor progression have been widely demonstrated in other cancers. For example, decreased exosomal miR-375-3p was detected in the plasma of diffuse large B-cell lymphoma patients (26), while higher expression of plasma miR-375 in prostate cancer has been identified as compared to benign prostate hyperplasia (27) and was related to poor overall survival (28). Combining four tumor-associated exosomal miRNAs including miR-375 could facilitate the early diagnosis of breast cancer patients (29). Besides, exosomal miR-375 secreted by Merkel cell carcinoma could induce fibroblast polarization to construct a pro-tumorigenic microenvironment by targeting RBPJ and p53 (30). Exosomal miR-375 derived from umbilical cord mesenchymal stem cells could inhibit esophageal squamous cell carcinoma progression via inhibiting ENAH (31). These researches underlined the importance of exosomal miR-375 in cell communications and tumor progressions, but its role in SCLC has never been explored.

In our study, we identified that SCLC-cell-derived miR-375-3p was unwrapped into exosomes and internalized by vascular endothelial cells to break vascular barriers by inhibiting tight junction (TJ) protein claudin-1. Our results uncovered the crucial roles of exosomal miR-375-3p in regulating vascular endothelial barrier integrity and SCLC metastasis, provided a potential candidate biomarker for the management of SCLC patients in the future. We present the following article in accordance with the ARRIVE reporting checklist (available at <https://dx.doi.org/10.21037/tlcr-21-356>).

## Methods

### *Patient samples*

Patient plasma or serum were obtained from SCLC or non-small cell lung cancer (NSCLC) patients who accepted surgery or tissue aspiration biopsy at the National Cancer Center (NCC)/National Clinical Research Center for Cancer/Cancer Hospital, Chinese Academy of Medical Sciences and Peking Union Medical College. Normal blood samples were obtained from healthy volunteers

who received medical examination in Cancer Prevention Department of NCC. Patients did not receive any antitumor therapeutics before blood sample collection. Medical ethics committee of NCC consented our protocol (NO. 20/250-2446). The study was conducted in accordance with the Declaration of Helsinki (as revised in 2013). Blood samples from three cohorts were included in this study: (I) Cohort 1 was used to discover the exosomal miRNAs that might play crucial roles in SCLC metastasis. Four pooled plasma samples were collected from 5 SCLC patients with distant metastasis (sample 1), 6 SCLC patients without distant metastasis (sample 2) and 11 healthy volunteers (samples 3 and 4). Exosomes were isolated from the four pooled plasma samples to conduct small RNA sequencing. (II) Cohort 2 included 57 SCLC patients and 25 healthy volunteers, from which plasma samples were collected to verify the dysregulation of miR-375-3p. (III) Cohort 3 included 69 SCLC patients, 46 NSCLC patients and 32 normal volunteers, from which serum samples were collected to evaluate the specificity of miR-375-3p in SCLC metastasis. All blood samples were obtained between August 2008 and December 2019. [Tables S1,S2](#) summarized the relevant clinical data of the patients.

#### ***Small RNA sequencing and exosome isolation and identification***

The details were shown in the Supplementary Methods ([Appendix 1](#)).

#### ***Exosome labeling and processing***

To assess the uptake of SCLC-cell-secreted exosomal miRNA in human umbilical vein vascular endothelial cells (HUVECs), Cy3-labeled miR-375-3p mimics were transfected into H446 cells, and the old culture medium (CM) was refreshed with CM containing exosome-depleted FBS for cell culture after 8 hours of transfection. Forty-eight hours later, exosomes in CM were collected by ultracentrifugation, followed by processing for PKH67 (Sigma) labeling. After washing with PBS once to remove excess dye, PKH67-labeled exosomes were harvested by ultracentrifugation and added to the CM of HUVECs. After incubation with PKH67-labeled exosomes for 12 hours, HUVECs were washed with PBS twice to remove excess exosomes followed by cell fixation using 4% paraformaldehyde solution. Cell nucleus of HUVECs were stained by DAPI and the uptake of exosomes in

HUVECs was observed under a fluorescence microscope. All steps were conducted in the dark to avoid fluorescence quenching.

To transfer the mimics or inhibitors of miR-375-3p directly into isolated exosomes, Exo-Fect Exosome Transfection Reagent (System Biosciences, cat. NO. EXFT20A-1) was applied following the instructions.

#### ***Cell lines and cell culture***

The H446 (HTB-171) and H1048 (CRL-5853) SCLC cell lines were purchased from the American Type Culture Collection (ATCC) and were maintained in ATCC recommended culture medium. HUVECs and HEK293T cells were cultured in DMEM (Corning) containing 10% FBS (Gibco) and 1% penicillin and streptomycin (Gibco).

#### ***Cell transfection and green fluorescent protein (GFP)<sup>+</sup> SCLC subline construction***

The mimics of miR-375-3p (miR-375, 5'-UUUGUUCGU UCGGCUCGCGUGA-3'), negative control mimics (NC, 5'-UUCUCCGAACGUGUCACGUTT-3'), the inhibitors of miR-375-3p (anti-miR-375, 5'-UCACGCG AGCCGAACGAACAAA-3') and negative control inhibitors (anti-NC, 5'-CAGUACUUUUGUGUAGUACAA-3') were synthesized in GenePharma (Shanghai, China). siRNAs targeting claudin-1 (siRNA-1, 5'-CAAUAGAA UCGUUCAAGAATT-3'; siRNA-2, 5'-ACGAUGAG GUGCAGAAGAATT-3'; siRNA-3, 5'-GGGCAGAU CCAGUGCAAAGTT-3'; siRNA-NC, 5'-UUCUCCGA ACGUGUCACGUTT-3') were purchased from SyngenTech (Beijing, China). Synthesized RNAs were transfected into SCLC cells or HUVECs with Lipofectamine RNAiMAX Transfection Reagent (Invitrogen) following the instructions. Claudin-1-expressing plasmid and the negative control plasmid were derived from Vigene Biosciences (Shandong, China) and transfected into HUVECs with Lipofectamine 3000 Transfection Reagent (Invitrogen).

To establish GFP<sup>+</sup> SCLC sublines, GFP-expressing plasmids purchased from Obio Technology (Shanghai, China) together with lentivirus packaging plasmids were transfected into HEK293T cells by Lipofectamine 3000 Transfection Reagent. Sixty hours later, lentivirus was harvested and concentrated to infect H446 cells. Infected H446 cells were screened with puromycin for two weeks to establish GFP<sup>+</sup> H446 sublines.

### **RNA isolation and qRT-PCR**

The details were shown in the Supplementary Methods (Appendix 1). Table S3 summarized associated primers.

### **Western blotting and cell immunofluorescence**

The details were shown in the Supplementary Methods (Appendix 1).

### **Tube formation and cell migration assays**

In tube formation assays,  $2 \times 10^4$  HUVECs were added in a 96-well plate per well which was pre-coated with 50  $\mu$ L Matrigel (Corning, cat. No. 354234) and cultured in a humidified incubator for 3 hours. Three hours later, the number of tubes formed per well was photographed under a microscope. In cell migration assays, HUVECs were digested from culture dishes, washed twice with medium without FBS and seeded on upper chambers of 24-well Transwell filters (Corning, 8  $\mu$ m, cat. NO. 3422) at a density of  $3 \times 10^4$  cells/well. Culture medium with 20% FBS was added to lower chambers. After migrating for 20 hours, migrated HUVECs were fixed using methanol, stained using Giemsa followed by photographing and counting.

### **In vitro permeability assay and transendothelial migration assay**

For the *in vitro* permeability assay,  $3 \times 10^4$  HUVECs were added to upper chambers of 24-well Transwell filters (Corning, 0.4  $\mu$ m, cat. NO. 3470) and treated with culture medium or exosomes from SCLC cells for 48 hours with HUVECs reaching 100% confluence. Fluorescein isothiocyanate-dextran (FITC-dextran, Sigma, cat. NO FD70S) was then added to upper chambers at 1 mg/mL. Medium in the lower chamber was collected at 30 min, 60 and 90 min successively, to detect its fluorescence intensity with 490 nm excitation and 520 nm emission.

For the transendothelial migration assay,  $3 \times 10^4$  HUVECs were seeded on upper chambers of 24-well Transwell filters (Corning, 8  $\mu$ m, cat. NO. 3422) and treated with SCLC-cell-derived exosomes for 48 hours. After the vascular endothelial cells reached 100% confluence, GFP<sup>+</sup> H446 cells were added in upper chambers ( $2 \times 10^4$  cells/well). Culture medium containing 20% FBS was added to lower chambers for transendothelial migration of GFP<sup>+</sup> H446 cells. After twelve hours of migration, cells remaining on

upper chambers were swabbed, cells migrated through filters were counted under a fluorescence microscope.

### **Liquid chromatography-mass spectrometry/mass spectrometry analysis (LC-MS/MS)**

The details were shown in the Supplementary Methods (Appendix 1).

### **Dual-luciferase reporter assay**

Potential target sequences of miR-375-3p in 3' UTR segment of claudin-1 together with mutant sequences were synthesized and inserted into the pGL3.0 vector. HUVECs were digested and placed in a 12-well plate one day before transfection and allowed to reach 40–50% confluence. Luciferase-expressing plasmids together with miR-375-3p mimics or negative control were transfected to HUVECs with Lipofectamine 3000 Transfection Reagent. Thirty-six to 48 hours later, the transfected HUVECs were harvested to determine the relative luciferase activity using Dual-Luciferase Reporter Assay System (Promega).

### **Animal experiments**

Animal experiments were performed under a project license (NO. NCC2020A292) granted by Animal Care and Use Committee of National Cancer Center/National Clinical Research Center for Cancer/Cancer Hospital, in compliance with institutional guidelines for the care and use of animals. BALB/c nude mice (female, 5-week-old) and NOD/SCID mice (female, 4-week-old) were obtained from HFK Bioscience (Beijing, China) and fed in a specific-pathogen-free environment.

For the *in vivo* permeability assays, a total of 24 BALB/c nude mice were randomly and equally divided into 4 groups: H446/NC-EXO, H446/miR-375-EXO, H1048/NC-EXO, H1048/miR-375-EXO. miR-375-3p-overexpressed exosomes (miR-375-EXO) or control exosomes (NC-EXO) were intraperitoneally injected into BALB/c nude mice twice a week. Two weeks later, exosome-treated mice were injected with FITC-dextran (100 mg/kg) via the tail vein and sacrificed after transcardiac perfusion for 2 hours. The lung, liver and brain tissues of mice were removed and stored at  $-80$  °C to make frozen sections by embedding in Tissue-Teck OCT compound (Sakura, Tokyo, Japan) for evaluating the leakage of FITC-dextran under a confocal microscope.

For the metastasis assay, a total of 24 NOD/SCID mice

were randomly divided into 4 groups, with 5 mice in H446/NC-EXO group, 5 mice in H446/miR-375-EXO, 7 mice in H1048/NC-EXO, and 7 mice in H1048/miR-375-EXO. NOD/SCID mice were intraperitoneally injected with miR-375-3p-overexpressing exosomes (miR-375-EXO) or control exosomes (NC-EXO) twice a week for 2 weeks followed by injection of  $5 \times 10^6$  wild type H446 or H1048 cells via tail veins. One mouse in H1048/miR-375-EXO group died while tail vein injecting. Two months later, mice were sacrificed by carbon dioxide anesthetization, and the lungs of the mice were removed for formalin fixation, paraffin sectioning and hematoxylin-eosin (HE) staining.

### Statistical analysis

We applied GraphPad Prism 6 software to conduct data analysis. Student's *t*-test was performed in assessing the differences between two groups while one-way ANOVA was conducted among more than two groups. Chi-square test was applied to evaluate relationships between miR-375-3p and clinical characteristics. All quantitative results are exhibited as the mean  $\pm$  SD.

## Results

### Exosomal miR-375-3p was upregulated in metastatic SCLC

To identify exosomal miRNAs that might promote SCLC metastasis, four pooled plasma of SCLC patients with or without metastasis or healthy volunteers (Table S1) were collected to isolate exosomes, extract exosomal RNA followed by small RNA sequencing. Exosomes isolated from plasma showed a specific exosomal morphology under transmission electron microscopy (TEM) (Figure 1A). Most exosomes had a diameter of approximately 100 nm, which was evaluated by nanoparticle tracking analysis (NTA) (Figure 1B). Two exosome-specific proteins, CD9 and TSG101, and one exosome-negative protein calnexin were detected in plasma exosomes by western blotting (WB) (Figure 1C). The small RNA sequencing results were used for differential expression analysis between SCLC patients and healthy volunteers as well as between metastatic SCLC and nonmetastatic SCLC. The most dysregulated miRNAs are listed in Figure 1D,E, miR-375-3p was upregulated in SCLC patients compared to healthy volunteers (Figure 1D) and in metastatic SCLC compared to nonmetastatic SCLC (Figure 1E). Considering that miR-375-3p was the most abundant miRNA in the plasma of SCLC patients (Figure 1F)

and its critical role in tumor progression has been reported in other tumors, we speculated that exosomal miR-375-3p might exert an important influence on the progress of SCLC metastasis.

To validate the results of RNA sequencing, another two groups of blood samples were used in this study (Table S2). qRT-PCR verified the obvious upregulation of miR-375-3p in plasma exosomes of 57 SCLC patients compared to that of 25 healthy volunteers (Figure 1G). Subgroup analysis found the upregulation of plasma exosomal miR-375-3p was mainly enriched in stage IV SCLC patients who had distant metastasis (Figure 1H). In concordance with the plasma results, the expression of serum miR-375-3p was also upregulated in 69 SCLC patients, especially in stage IV SCLC patients, compared with 32 normal volunteers (Figure 1I,J). Interestingly, no variation of serum miR-375-3p was found in 46 NSCLC patients, which indicated the potential specific function of miR-375-3p in SCLC metastasis (Figure 1I). Moreover, clinical relevance analysis revealed the level of exosomal miR-375-3p was statistically related to tumor size, lymph node metastasis, distant metastasis and TNM stages in SCLC patients (Tables 1,2).

### SCLC-cell secreted exosomal miR-375-3p was delivered to HUVECs

Growing evidence has shown that the miRNAs of exosomes can promote metastasis by targeting vascular endothelial cells to facilitate angiogenesis or induce vascular permeability (23-25). Thus, we focused on vascular endothelial cells to investigate whether exosomal miR-375-3p could be transferred to endothelial cells to further facilitate SCLC metastasis by influencing their biological functions.

First, the level of miR-375-3p in several SCLC cells were detected. H446 and H1048, which had a low endogenous expression of miR-375-3p in both their cells and their cell-secreted exosomes (Figure S1A and S1B), were chosen to construct SCLC sublines with miR-375-3p overexpression. SCLC-cell-secreted exosomes extracted from culture medium were identified by TEM, NTA and WB (Figure S1C,D,E). miR-375-3p mimics were transfected to H446 and H1048 cells to upregulate miR-375-3p. qRT-PCR confirmed the overexpression of miR-375-3p in both cells and cell-secreted exosomes (Figure 2A, Figure S2A). Then, miR-375-3p-overexpressed exosomes (miR-375-EXO) or negative control exosomes (NC-EXO) were incubated with HUVECs. After incubation with miR-375-EXO,

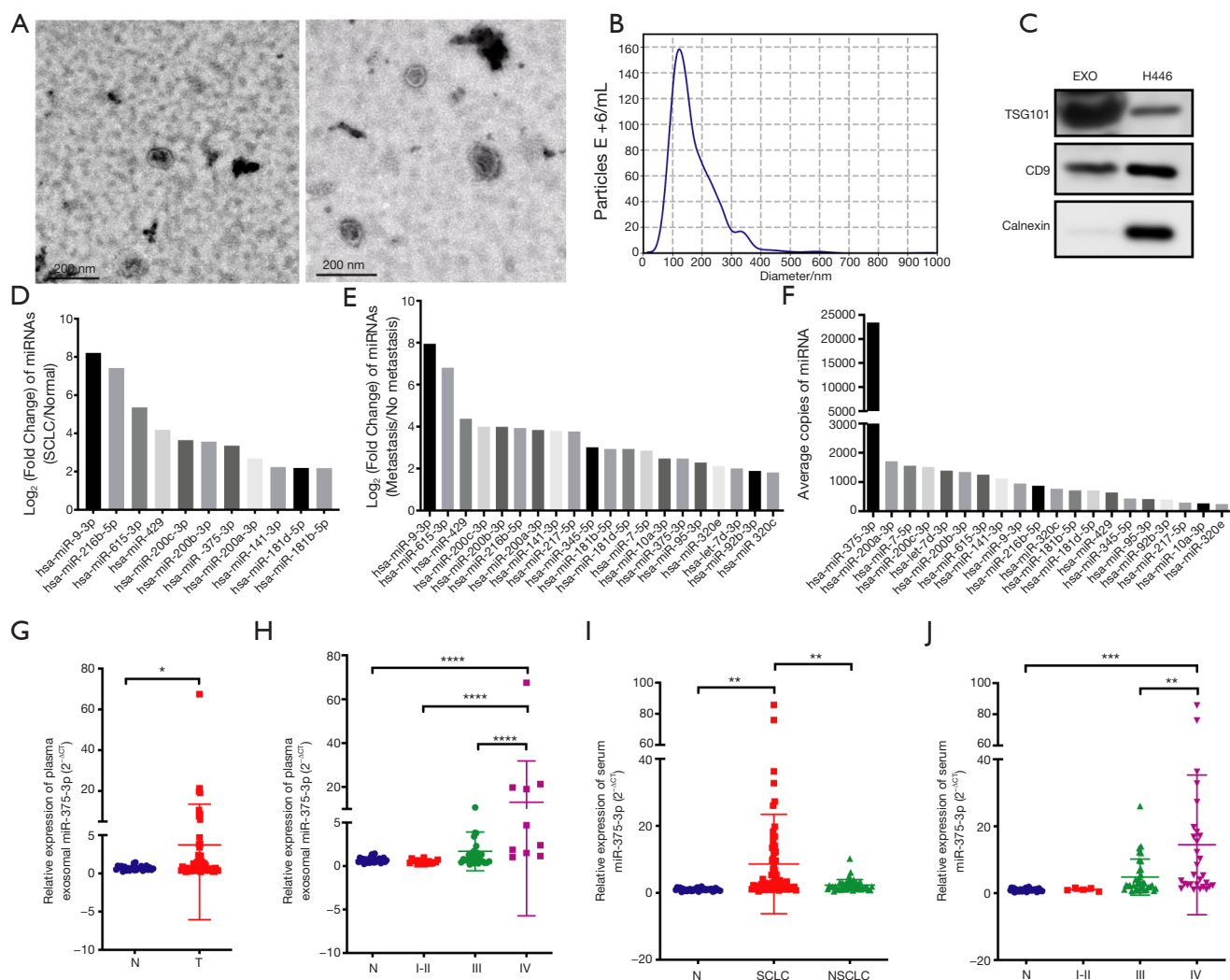


**Figure 1** The level of exosomal miR-375-3p was obviously upregulated in SCLC patients. (A) Representative TEM images of plasma exosomes of SCLC patients. (B) Diameter and concentration of plasma exosomes determined by NTA. (C) Detection of TSG101, CD9 and calnexin in plasma exosomes using western blotting. (D) Differentially expressed exosomal miRNAs in pooled plasma of SCLC patients compared with healthy volunteers. (E) Differentially expressed exosomal miRNAs in pooled plasma of SCLC patients with metastasis compared with whom without metastasis. (F) Average copies of exosomal miRNAs in four pooled plasma samples. (G,H) Relative expression of plasma exosomal miR-375-3p in cohort 2. (I,J) Relative expression of serum miR-375-3p in cohort 3. SCLC, small cell lung cancer; NSCLC, non-small cell lung cancer; N, normal; T, tumor; EXO, exosomes. \*,  $P < 0.05$ ; \*\*,  $P < 0.01$ ; \*\*\*,  $P < 0.001$ ; \*\*\*\*,  $P < 0.0001$ .

the expression of miR-375-3p was upregulated at 4 hours and reached a peak at 12 hours in HUVECs (Figure 2B, Figure S2B), with no changes in the level of pri-miR-375 (Figure 2C). Besides, the upregulated miR-375-3p in HUVECs could be abrogated by pretreating exosomes with the inhibitor of exosome internalization Annexin V but could not be influenced by 5,6-dichloro-1- $\beta$ -D-ribofuranosylbenzimidazole (DRB), an inhibitor of RNA transcription (Figure 2D). These results revealed that the

upregulated miR-375-3p in HUVECs was due to the uptake of exosomes rather than the processing of pri-miRNA.

To visualize the delivery of exosomal miR-375-3p directly, Cy3-labeled miR-375-3p mimics were transfected into H446 cells followed by exosome isolation and PKH67 labeling. Labeled exosomes were incubated with HUVECs for 12 hours. The presence of HUVECs was examined under a fluorescence microscope, and both the red fluorescence of Cy3 and the green fluorescence of PKH67

**Table 1** The correlations of the plasma exosomal miR-375-3p level with SCLC clinical features in cohort 2

Clinical features	Group	Low miR-375-3p expression	High miR-375-3p expression	P value
Sex	Female	12	10	0.5162
	Male	16	19	
Age	<60	16	13	0.3525
	≥60	12	16	
T	T1-T2	20	6	0.0001***
	T3-T4	8	23	
N	N0-N1	17	2	<0.0001****
	N2-N3	11	27	
M	M0	28	17	0.0001***
	M1	0	12	
Stage	I-II	15	2	0.0001***
	III-IV	13	27	

SCLC, small cell lung cancer; T, tumor; N, node; M, metastasis. \*\*\*, P<0.001; \*\*\*\*, P<0.0001.

**Table 2** The correlations of the serum miR-375-3p level with SCLC clinical features in cohort 3

Clinical features	Group	Low miR-375-3p expression	High miR-375-3p expression	P value
Sex	Female	6	8	0.5906
	Male	28	27	
Age	<60	14	14	0.9207
	≥60	20	21	
T	T1-T2	19	9	0.0107*
	T3-T4	15	26	
N	N0-N1	9	1	0.0053**
	N2-N3	25	34	
M	M0	23	17	0.1085
	M1	11	18	
Stage	I-II	5	0	0.0185*
	III-IV	29	35	

SCLC, small cell lung cancer; T, tumor; N, node; M, metastasis. \*, P<0.05; \*\*, P<0.01.

were observed in exosome-treated HUVECs (*Figure 2E*), which confirmed that miR-375-3p could be delivered into HUVECs via SCLC-cell-secreted exosomes.

#### ***Exosomal miR-375-3p increased vascular permeability and promoted SCLC cell transendothelial migration in vitro***

To figure out the influences of miR-375-3p on HUVECs,

we transfected miR-375-3p mimics (miR-375) or negative control mimics (NC) into HUVECs and explored their effects on the biological functions of HUVECs. The upregulation of miR-375-3p in HUVECs after transfection with miR-375 was validated by qRT-PCR (*Figure S3A*). Interestingly, compared with the NC group, HUVECs transfected with miR-375 showed no alterations in cell migration (*Figure S3B*) but had decreased tube formation

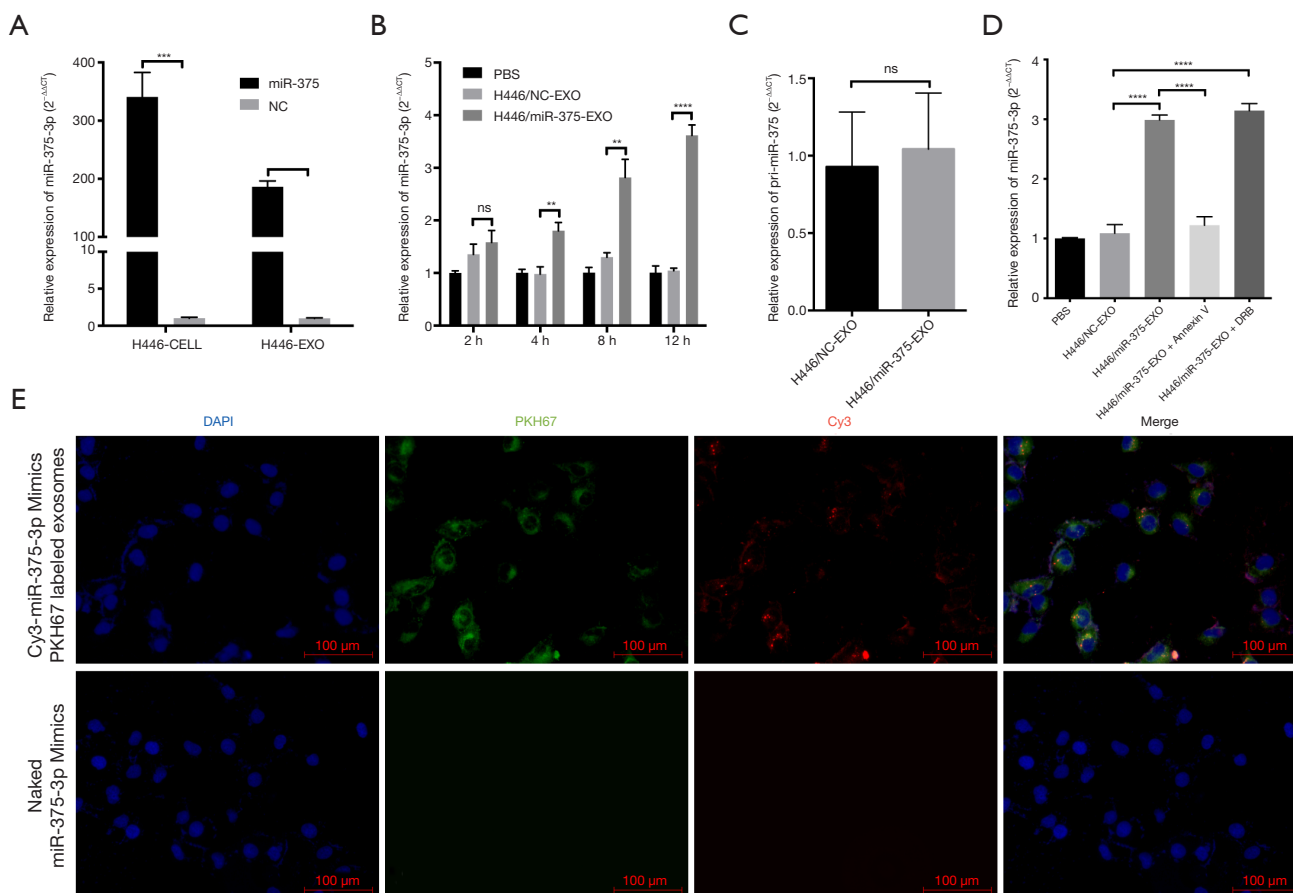


**Figure 2** SCLC-cell-secreted miR-375-3p was delivered to HUVECs via exosomes. (A) Expression of miR-375-3p in H446 cells or H446-cell-derived exosomes after transfection with miR-375-3p mimics (miR-375) or negative control mimics (NC). (B) Expression of miR-375-3p in HUVECs after treatment with H446/miR-375-EXO or H446/NC-EXO for 2, 4, 8 and 12 hours. (C) Expression of pri-miR-375 in HUVECs after incubation with H446/miR-375-EXO or H446/NC-EXO for 12 hours. (D) Level of miR-375-3p in HUVECs or DRB-pretreated HUVECs after incubation with H446/NC-EXO, H446/miR-375-EXO or Annexin V-blocked H446/miR-375-EXO. (E) Representative images of HUVECs under a fluorescence microscope, the upper panel showed the presence of HUVECs incubated with PKH67-labeled exosomes secreted by CY3-miR-375-3p mimic-transfected H446 cells, the lower panel showed the presence of HUVECs treated with naked-CY3-miR-375-3p mimics. EXO, exosomes; DRB, 5,6-dichloro-1- $\beta$ -D-ribofuranosylbenzimidazole; PBS, phosphate buffer saline; H446/miR-375-EXO, exosomes derived from miR-375-transfected H446 cells; H446/NC-EXO, exosomes derived from NC-transfected H446 cells; h, hours; ns, not significant. \*\*,  $P < 0.01$ ; \*\*\*,  $P < 0.001$ ; \*\*\*\*,  $P < 0.0001$ .

capacity (Figure S3C) and prominently increased cell permeability (Figure S3D), which might facilitate the invasion of tumor cells. Transendothelial migration assays confirmed that more SCLC cells migrated through miR-375-transfected HUVEC monolayers than NC-transfected HUVEC monolayers (Figure S3E). Thus, we speculated that miR-375-3p might facilitate SCLC metastasis by broking the vascular endothelial barriers rather than affecting angiogenesis.

We then treated HUVECs with culture medium (CM)

or exosomes (EXO) obtained from miR-375- or NC-transfected H446 or H1048 cells to evaluate their influence on vascular endothelial barriers. As expected, compared with the negative control groups (NC-CM or NC-EXO), miR-375-3p-overexpressed CM or exosomes (miR-375-CM, miR-375-EXO) induced the leakage of monolayer vascular endothelial cells, and the increased permeability could be rescued by pretreating exosomes with Annexin V (Figure 3A,B and Figure S4A,B). Pre-transfecting HUVECs with the inhibitors of miR-375-3p (anti-

miR-375) also reversed the increased permeability induced by miR-375-EXO (Figure 3C and Figure S4C). Moreover, transendothelial migration assay showed that more SCLC cells migrated through miR-375-EXO-treated HUVEC monolayers than NC-EXO-treated HUVEC monolayers (Figure 3D and Figure S4D), and pretreating exosomes with Annexin V or pre-transfecting HUVECs with anti-miR-375 abrogated the promoting function of miR-375-EXO on transendothelial migration assays (Figure 3D,E and Figure S4D,E).

To further validate the influence of exosomal miR-375-3p on vascular endothelial cells, we loaded miR-375-3p mimics into NC-EXO or loaded miR-375-3p inhibitors into miR-375-EXO to enhance or block the effect of exosomal miR-375-3p, respectively. As shown in Figure 3F,G and Figure S4F,G, treating HUVECs with miR-375-3p-mimic-loaded NC-EXO (NC-EXO+miR-375) increased HUVECs-monolayer permeabilities and promoted the migration of SCLC cells through HUVEC monolayers, while treating HUVECs with miR-375-3p-inhibitor-loaded miR-375-EXO (miR-375-EXO+anti-miR-375) reversed the increased permeabilities of HUVECs and reduced the number of SCLC cells that migrated through HUVEC monolayers. All of the above results demonstrated that exosomal miR-375-3p secreted by SCLC cells could induce the permeability of vascular endothelial cells and promote SCLC cell migration through vascular endothelial barriers *in vitro*.

#### ***SCLC-cell-secreted miR-375-3p induced blood vessel permeability in vivo***

To clarify the role of miR-375-3p-enriched exosomes on blood vessel walls *in vivo*, BALB/c nude mice were treated with exosomes derived from miR-375-3p-mimic-transfected H446 or H1048 cells or control cells (miR-375-EXO or NC-EXO) two times per week for 2 weeks. Before mice sacrificing, FITC-dextran were injected via the tail vein, and the lung, liver and brain tissues of mice were removed to assess the leakage of FITC-dextran under a confocal microscope. As shown in Figure 4A and Figure S5A, compared with that in NC-EXO-treated mice, the amount of FITC-dextran that infiltrated from blood vessels into lung tissues was significantly increased in miR-375-EXO-treated mice. Moreover, the liver and brain tissues in miR-375-EXO-treated mice also showed more FITC-dextran infiltration than NC-EXO-treated mice (Figure 4B,C and Figure S5B,C). These results

implied that SCLC-cell-derived miR-375-3p might be transferred to different organs to increase the permeability of blood vessel walls *in vivo*.

#### ***miR-375-3p increased HUVEC permeabilities by inhibiting TJ protein claudin-1***

To excavate the potential downstream pathways of miR-375-3p, we compared the protein components of miR-375-3p-overexpressed or control HUVECs using protein mass spectrometry analysis. A total of 83 upregulated proteins and 90 downregulated proteins (Figure S6A,B, Table S4) were identified. Gene Ontology (GO) enrichment analysis found the dysregulated proteins were mostly located on the intermediate filament cytoskeleton, intermediate filaments and cell-cell junctions (Figure S6C). TJs are the main component of vascular endothelial cell-cell junctions, which serve as gatekeepers to control the infiltration of cells and solutes through the walls of blood vessels and are necessary in maintaining the integrity of blood vessel walls (32). The destruction of TJs destroys the integrity of blood vessel barriers, leads to increased paracellular permeability and promotes the metastasis of various cancers by facilitating the transendothelial invasion of tumor cells (33). Therefore, we focused on TJ proteins to study the downstream pathways of miR-375-3p.

Claudin-11 and claudin-1, two essential proteins of TJs, were identified by protein mass spectrometry analysis to be downregulated in HUVECs after transfection with miR-375-3p mimics (Table S4). Then, we validated the expressions of claudin-11 and claudin-1 utilizing qRT-PCR and WB. As shown in Figure 5A,B,C, both RNA and protein levels of claudin-11 in HUVECs were not changed (Figure 5A) while claudin-1 was significantly downregulated at both the RNA and protein levels (Figure 5B,C) after miR-375-3p overexpression. Considering that a previous study documented that claudin-1 was directly targeted by miR-375 (34), we suspected miR-375-3p induced the permeability of HUVECs by regulating the expression of the TJ protein claudin-1.

Sequence similarity analysis identified that the sequences of miR-375-3p in human and mouse were homologous (Figure 5D). Next, basing on predicted target sites (TS) of miR-375-3p in the 3' UTR of claudin-1, plasmids with wild type (WT) or mutant TS were constructed (Figure 5D) to conducted a dual-luciferase assay. As shown in Figure 5E, miR-375-3p inhibited the luciferase activity of plasmids containing WT sequences, and this inhibition was

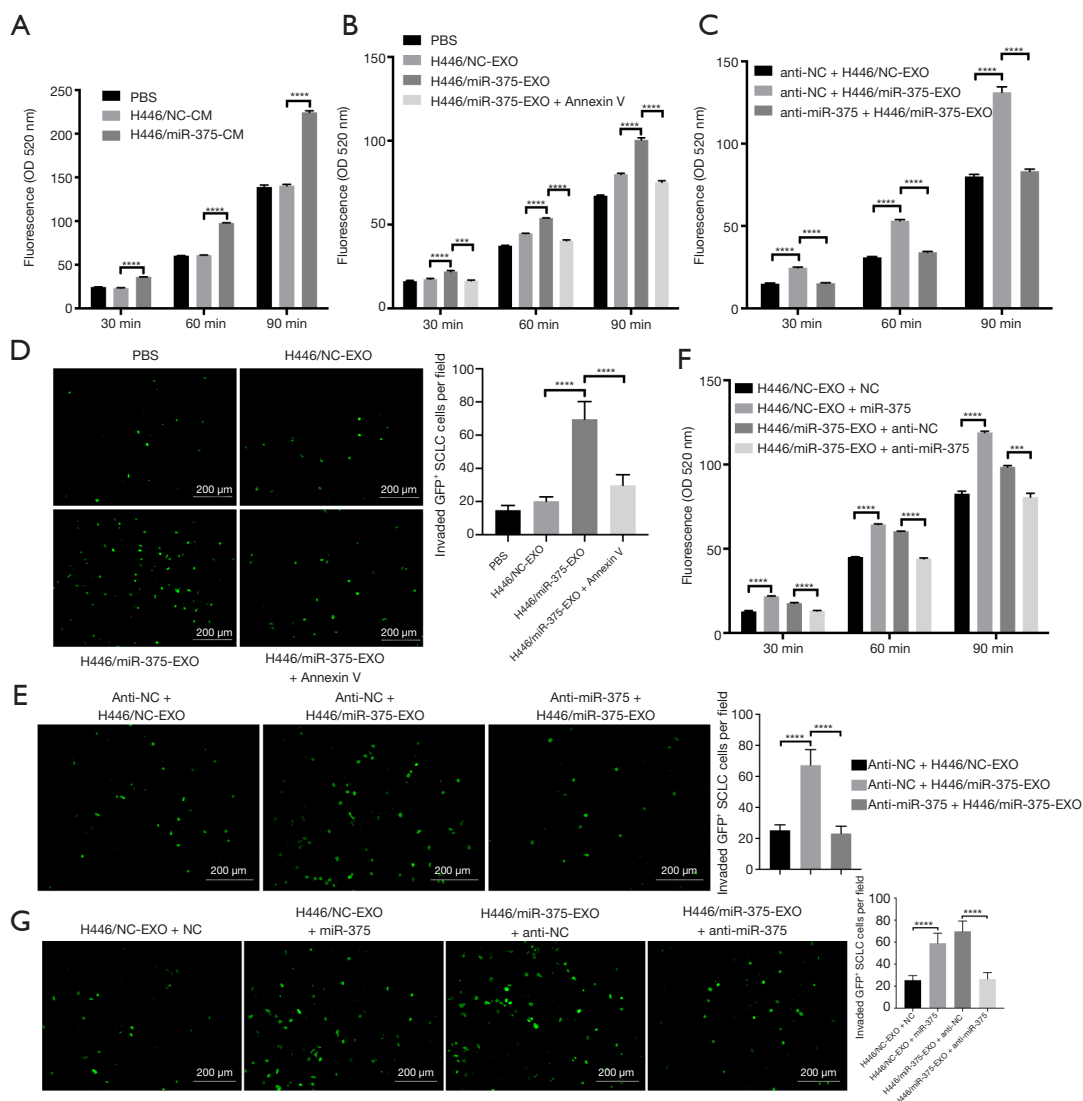


**Figure 3** Exosomal miR-375-3p secreted by H446 cells induced the permeability of HUVECs and promoted SCLC cell transendothelial migration *in vitro*. (A) Fluorescence intensity of FITC-dextran passing through HUVEC monolayers treated with H446/miR-375-CM or H446/NC-CM. (B) Fluorescence intensity of FITC-dextran passing through HUVEC monolayers treated with H446/miR-375-EXO, H446/NC-EXO or Annexin V-blocked H446/miR-375-EXO. (C) Fluorescence intensity of FITC-dextran passing through H446/miR-375-EXO- or H446/NC-EXO-treated HUVEC monolayers pre-transfected with anti-miR-375 or anti-NC. (D) Representative images of GFP+ SCLC cells migrated through H446/miR-375-EXO- or H446/NC-EXO-treated HUVEC monolayers, the green spots in the images indicated the migrated GFP+ SCLC cells, the right bar chart indicated the number of migrated cells. (E) Representative images of GFP+ SCLC cells migrated through H446/miR-375-EXO- or H446/NC-EXO-treated HUVEC monolayers pre-transfected with anti-miR-375 or anti-NC; the right bar chart indicated the number of migrated cells. (F) Fluorescence intensity of FITC-dextran passing through HUVEC monolayers treated with miR-375-3p-mimic-loaded H446/NC-EXO or miR-375-3p-inhibitor-loaded H446/miR-375-EXO. (G) Representative images of GFP+ SCLC cells that migrated through HUVEC monolayers treated with miR-375-3p-mimic-loaded H446/NC-EXO or miR-375-3p-inhibitor-loaded H446/miR-375-EXO, the right bar chart indicated the number of migrated cells. SCLC, small cell lung cancer; GFP, green fluorescent protein; PBS, phosphate buffer saline; H446/miR-375-CM, culture medium derived from miR-375-transfected H446 cells; H446/NC-CM, culture medium derived from NC-transfected H446 cells; H446/miR-375-EXO, exosomes derived from miR-375-transfected H446 cells; H446/NC-EXO, exosomes derived from NC-transfected H446 cells; anti-miR-375, miR-375-3p inhibitors; anti-NC, negative control inhibitors. \*\*\*,  $P < 0.001$ ; \*\*\*\*,  $P < 0.0001$ .

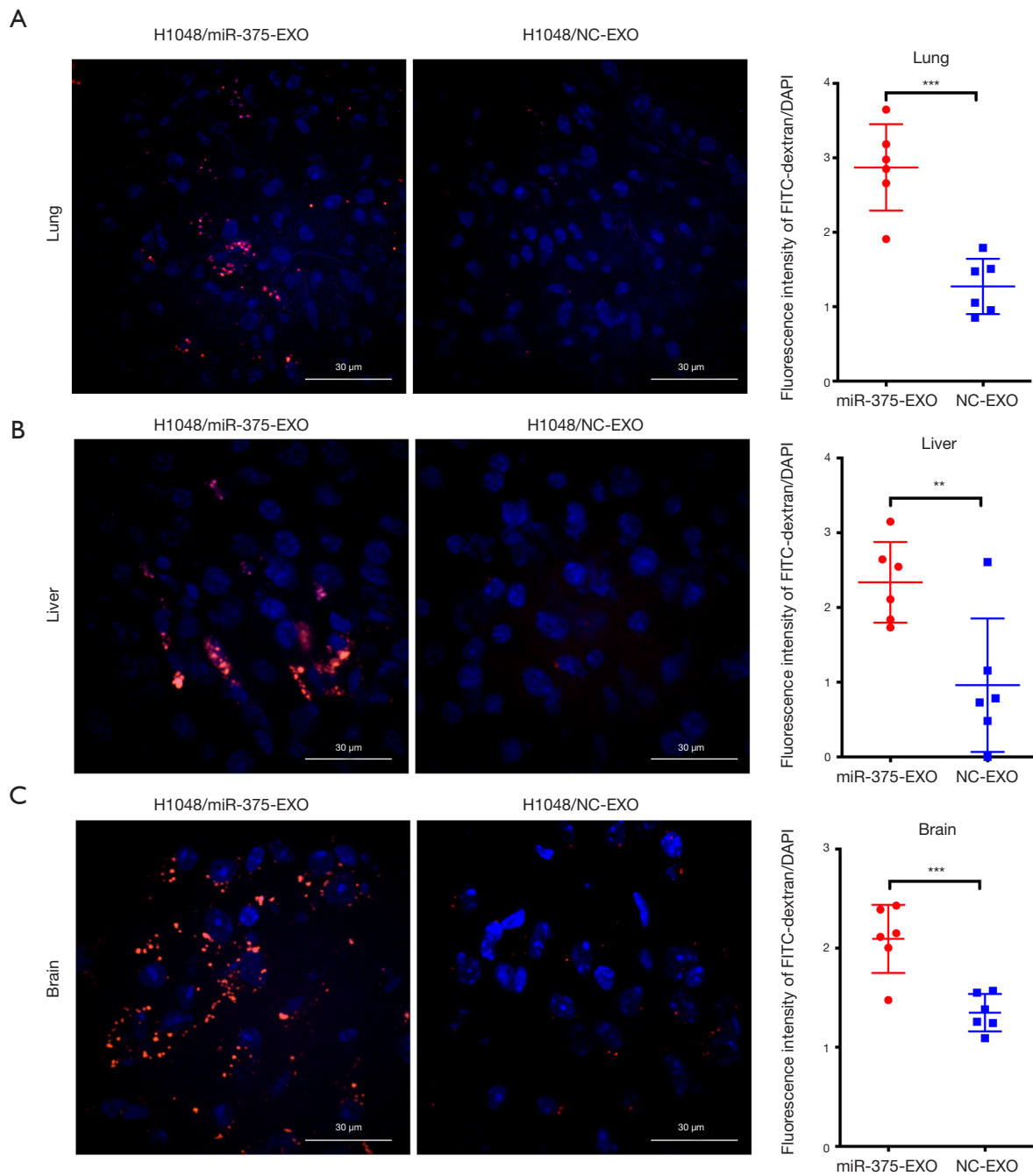


**Figure 4** H1048-cell-derived exosomal miR-375-3p induced the permeability of blood vessels *in vivo*. (A-C) Typical images of infiltrated FITC-dextran in the lung (A), liver (B) and brain (C) tissues of mice after treatment with H1048/miR-375-EXO or H1048/NC-EXO, with the red fluorescence indicating the infiltrated FITC-dextran, the blue fluorescence indicating the nucleus of cells and the right bar chart indicating the relative fluorescence intensity. FITC, fluorescein isothiocyanate; H1048/miR-375-EXO, exosomes derived from miR-375-transfected H1048 cells; H1048/NC-EXO, exosomes derived from NC-transfected H1048 cells. \*\*, P<0.01; \*\*\*, P<0.001.

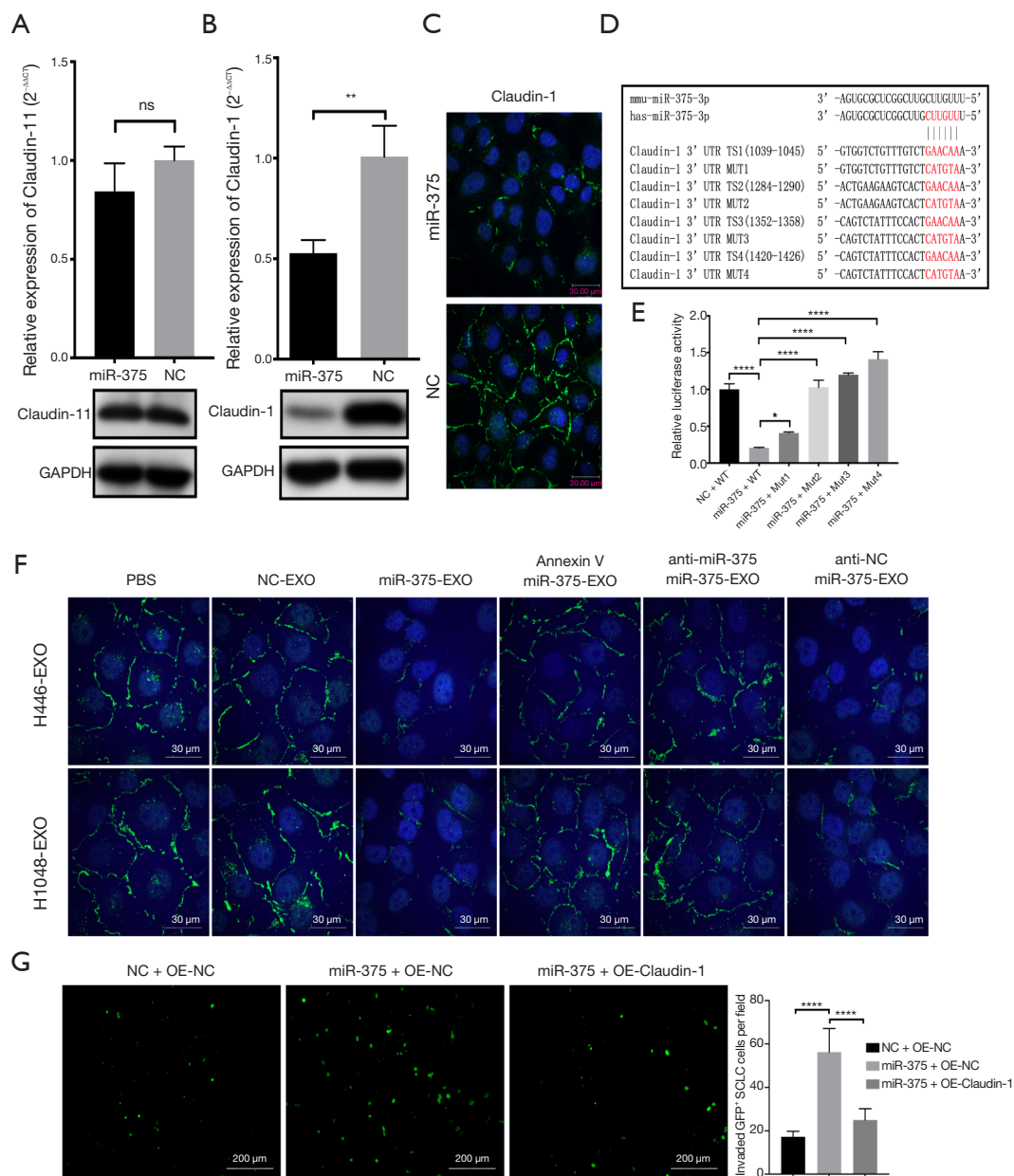


**Figure 5** miR-375-3p destroyed the integrity of blood vessels by inhibiting the TJ protein claudin-1. (A) The RNA and protein expressions of claudin-11 in miR-375-3p mimics (miR-375) or negative control mimics (NC) transfected HUVECs. (B) Both RNA and protein levels of claudin-1 decreased in miR-375-transfected HUVECs. (C) Representative immunofluorescence staining of claudin-1 in miR-375- or NC-transfected HUVECs. (D) The wild type or mutant predicted targeting sites of miR-375-3p in the 3'UTR of claudin-1. (E) The relative luciferase activity of HUVECs co-transfected with miR-375-3p mimics and wild type plasmids (miR-375 + WT) was dramatically decreased compared to that of those co-transfected with negative control mimics and wild type plasmids (NC + WT), and the inhibition of luciferase activity was abrogated by the mutation of targeting sequences (Mut1, Mut2, Mut3 and Mut4). (F) Representative immunofluorescence staining of claudin-1 in HUVECs after incubation with PBS, NC-EXO, miR-375-EXO or Annexin V-blocked miR-375-EXO, as well as in HUVECs pre-transfected with anti-miR-375 or anti-NC and incubated with miR-375-EXO. (G) The transendothelial migration of GFP + SCLC cells induced by miR-375-3p was abrogated by overexpressing claudin-1 in HUVECs. 3'UTR, 3' untranslated regions; TS, target site; MUT, mutant; OE, overexpression; PBS, phosphate buffer saline; anti-miR-375, miR-375-3p inhibitors; anti-NC, negative control inhibitors; ns, not significant. \*,  $P < 0.05$ ; \*\*,  $P < 0.01$ ; \*\*\*\*,  $P < 0.0001$ .

abrogated by the mutation of several target sites. Then, we explored whether the expression of claudin-1 could be inhibited by miR-375-3p-enriched exosomes. As shown in *Figure 5F* and *Figure S6D*, the level of claudin-1 in HUVECs was downregulated after treatment with miR-375-EXO, and the decrease in claudin-1 could be rescued when the absorption of miR-375-EXO was inhibited by Annexin V. Moreover, treating HUVECs with miR-375-3p-mimic-loaded NC-EXO (NC-EXO + miR-375) could also inhibit the expression of claudin-1, and treating HUVECs with miR-375-3p-inhibitor-loaded miR-375-EXO (miR-375-EXO + anti-miR-375) could reverse the downregulation of claudin-1 induced by miR-375-EXO (*Figure S6E*). In addition, when HUVECs were pre-transfected with the inhibitors of miR-375-3p (anti-miR-375), the downregulation of claudin-1 induced by miR-375-EXO could also be reversed (*Figure 5F* and *Figure S6F*). All of the above results validated miR-375-3p in SCLC-cell-secreted exosomes downregulated TJ protein claudin-1 in HUVECs.

To further clarify the function of claudin-1 in maintaining the integrity and permeability of HUVEC monolayers, we downregulated the level of claudin-1 in HUVECs using claudin-1-specific siRNAs (*Figure S7A*). The results showed that the downregulation of claudin-1 in HUVECs led to increased permeabilities of HUVEC monolayers (*Figure S7B*). Moreover, the increased permeability of HUVEC monolayers induced by miR-375-3p could be reversed by upregulation of claudin-1 (*Figure S7C*). Transendothelial migration assays also confirmed that knocking down the expression of claudin-1 could increase the number of SCLC cells that migrated through HUVEC monolayers (*Figure S7D*), while overexpressing claudin-1 could abrogate the promoting role of miR-375-3p on transendothelial migration assays (*Figure 5G*). All of the above results indicate miR-375-3p promotes the permeability of HUVECs by directly regulating the TJ protein claudin-1.

#### ***Exosomal miR-375-3p promoted SCLC metastasis in mice***

We have determined exosomal miR-375-3p secreted by SCLC cells could disrupt the vascular endothelial barrier and induce the permeability of blood vessels with an *in vivo* permeability assay; however, whether it can promote SCLC metastasis *in vivo* is still unknown. Thus, we treated NOD/SCID mice with NC-EXO or miR-375-EXO twice a week for two weeks followed by injecting with wild type H446 or

H1048 cells via the tail vein. Two months later, mouse lung tissues were fetched to evaluate the metastasis of SCLC. As shown in *Figure 6A,B*, in H446 cell-injected mice, 3 out of 5 (60%) mice showed lung metastasis in the H446/miR-375-EXO-treated group, while 0 out of 5 (0%) mice showed lung metastasis in the H446/NC-EXO-treated group. The number of metastatic nodules was also higher in the H446/miR-375-EXO-treated group than in the H446/NC-EXO-treated group, although the p value indicated no statistical significance (*Figure 6C*). Consistent with the results in H446 cell-injected mice, in H1048 cell-injected mice, 5 out of 6 (83.3%) mice showed lung metastasis in the H1048/miR-375-EXO-treated group, while 2 out of 7 (28.6%) mice showed lung metastasis in the H1048/NC-EXO-treated group (*Figure 6D,E*); the number of metastatic nodules was also significantly increased in the H1048/miR-375-EXO-treated group compared to that in the H1048/NC-EXO-treated group (*Figure 6F*). All of the above implied SCLC-cell-secreted exosomal miR-375-3p could facilitate SCLC metastasis *in vivo*.

## **Discussion**

In this study, exosomal miR-375-3p was discovered to be a critical regulator in SCLC metastasis for the first time. miR-375 was firstly characterized to be a conserved and pancreatic islet-specific miRNA regulating insulin secretion (35). In recent years, the downregulation and tumor suppressing role of miR-375 have been widely documented in different cancer types (36), including esophageal carcinoma (37), hepatoma (38), gastric cancer (39), head and neck cancer (40), glioma (41) and melanoma (42). Despite its significant tumor suppressive effect in multiple cancers, miR-375 was reported to be elevated to serve as an oncogenic regulator in breast (43) and prostate cancers (44). MiR-375 enriched in exosomes has also shown a great promise to be a liquid biomarker in the diagnosis and prognosis of human cancers such as breast cancer (29) and prostate cancer (27). Considering that the function of miRNA relies on the cellular context and tumor microenvironment, it is reasonable that miR-375 shows diverse functions in different cancers. However, how miR-375 functions in SCLC is ill-defined. Here, we showed the expression of exosomal miR-375-3p in SCLC patients was upregulated compared with that in healthy volunteers and that high miR-375-3p level was significantly associated with SCLC metastasis, which underlined the possible importance of miR-375-3p in SCLC malignancy. Moreover,

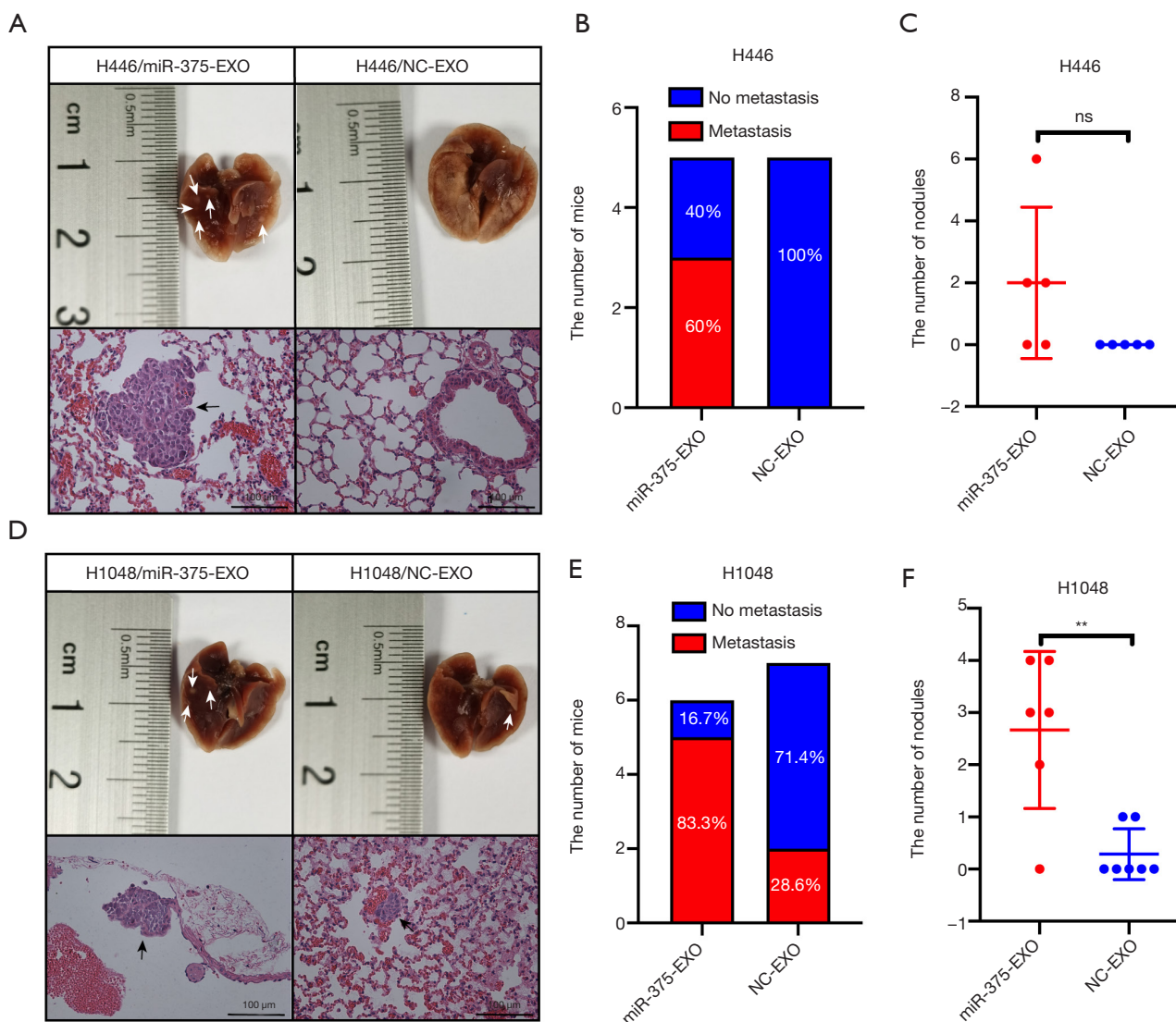


**Figure 6** Exosomal miR-375-3p promoted SCLC metastasis in mice. (A) The representative macrographs and HE images of the lungs of mice which were treated with H446/miR-375-EXO or H446/NC-EXO followed by injecting with wild type H446 cells via the tail vein. (B) The number of mice with or without lung metastasis in the H446/miR-375-EXO- or H446/NC-EXO-treated group. (C) The number of tumor nodules in the lung of mice which were treated with H446/miR-375-EXO or H446/NC-EXO. (D) The representative macrographs and HE images of lungs in mice which were treated with H1048/miR-375-EXO or H1048/NC-EXO followed by injecting with wild type H1048 cells via the tail vein. (E) The number of mice with or without lung metastasis in the H1048/miR-375-EXO- or H1048/NC-EXO-treated group. (F) The number of tumor nodules in the lungs of mice treated with H1048/miR-375-EXO or H1048/NC-EXO. H446/miR-375-EXO, exosomes derived from miR-375-transfected H446 cells; H446/NC-EXO, exosomes derived from NC-transfected H446 cells; H1048/miR-375-EXO, exosomes derived from miR-375-transfected H1048 cells; H1048/NC-EXO, exosomes derived from NC-transfected H1048 cells; ns, not significant. \*\*,  $P < 0.01$ .

we discovered the difference of miR-375-3p between NSCLC patients and normal volunteers was not statistically significant, which implied that miR-375-3p played a specific role in SCLC that it does not play in NSCLC. In fact, it

has been reported that miR-375 was differentially expressed between SCLC and NSCLC, and it was a potential biomarker discriminating SCLC from NSCLC (45). Interestingly, the expression of miR-375 was found to be

induced by the transcription factor ASH1, which is a critical regulator of lung cancer with neuroendocrine features (46). SCLC is the major subtype of lung neuroendocrine tumors, and approximately three-quarters of SCLC patients express ASH1 to support tumor cell growth and survival (47), which might explain the elevated level of miR-375-3p in SCLC patients. Recently, a novel model of SCLC molecular subtypes was established basing on the level of four key transcription regulators, including ASH1 (48), whether ASH1-subtype SCLC shows higher expression of miR-375-3p and more metastasis than other subtypes needs to be further explored.

Exosomes have been widely identified as nanoscale carriers mediating crosstalk among tumor cells and microenvironments, which contributes to premetastatic niche formation and finally tumor metastasis (49). For example, CEMIP-enriched exosomes were delivered to brain endothelial and microglial cells to support brain metastasis progression by producing proinflammatory cytokines (50). Colorectal cancer cell-secreted exosomal miRNAs are internalized by macrophages to induce M2 polarization via PTEN and promote liver metastasis of colorectal cancer (51). Exosomes secreted from HeLa cells can destroy endothelial barriers to facilitate tumor metastasis by inducing endoplasmic reticulum stress in endothelial cells (52). Exosomal miR-375 has also been validated to serve as a communicator mediating the crosstalk between different cells in the tumor microenvironment, thus affected the biological functions of exosome-recipient cells such as tumor cells (31) and fibroblasts (30). In our research, we revealed that miR-375-3p was enwrapped into exosomes by SCLC cells and delivered to vascular endothelial cells, and this communication was visualized under a fluorescence microscope. HUVECs treated by miR-375-3p-enriched exosomes showed increased permeability *in vitro*. Protein mass spectrometry analysis identified that proteins affected by miR-375-3p were mainly enriched in cell-cell junctions and that miR-375-3p reduced the integrity of vascular barriers by inhibiting the TJ protein claudin-1. Vascular endothelial cells are critical stromal cells that stabilize the tissue microenvironment by relying mainly on cell-cell junctions, especially TJs (32). The disruption of TJs between endothelial cells facilitates tumor cell transendothelial migration and further localization into distant metastatic sites. For example, exosomal miR-25-3p disrupts endothelial junctions by downregulating ZO-1, Occludin and claudin-5 and promotes colorectal cancer metastasis (24). The metastasis of hepatoma is induced

by exosomal miR-103, which breaks down endothelial barriers by attenuating VE-cadherin, p120 and ZO-1 (25). miR-105 in breast cancer cell-derived exosomes destroys endothelial junctions and contribute to tumor metastasis by inhibiting ZO-1 (23). In our results, another TJ protein, claudin-1, was found to be the critical endothelial junction protein regulated by miR-375-3p, and exosomal miR-375-3p secreted from SCLC cells destroyed endothelial barriers by directly downregulating the expression of claudin-1. Claudin-1 was previously found to be one of the downstream genes of miR-375, which facilitated NSCLC cell migration and invasion by regulating claudin-1 (34). However, our study was the first to determine exosomal miR-375/claudin-1 pathway in endothelial barrier maintenance and tumor metastasis.

Taken together, our research revealed that miR-375-3p-enriched exosomes secreted by SCLC could destroy blood barriers by targeting the vascular TJ protein claudin-1 to facilitate SCLC metastasis. This is the first study to explore metastasis-associated exosomal miRNAs in SCLC patients basing on small RNA omics, which was meaningful in the biomarker exploration of SCLC metastasis and lay a foundation for the future investigations of exosomal miRNAs in the progress of SCLC metastasis.

## Acknowledgments

*Funding:* This work was supported by the CAMS Innovation Fund for Medical Sciences (2016-I2M-1-001, 2017-I2M-1-005), the National Natural Science Foundation of China (81802299, 81502514), the Fundamental Research Funds for the Central Universities (3332018070), the National Key Basic Research Development Plan (2018YFC1312105), the National Key Research and Development Program of China (2016YFC0901401) and the Natural Science Foundation of Beijing (7214248).

## Footnote

*Reporting Checklist:* The authors have completed the ARRIVE reporting checklist. Available at <https://dx.doi.org/10.21037/tlcr-21-356>

*Data Sharing Statement:* Available at <https://dx.doi.org/10.21037/tlcr-21-356>

*Peer Review File:* Available at <https://dx.doi.org/10.21037/tlcr-21-356>

*Conflicts of Interest:* All authors have completed the ICMJE uniform disclosure form (available at <https://dx.doi.org/10.21037/tlcr-21-356>). The authors have no conflicts of interest to declare.

*Ethical Statement:* The authors are accountable for all aspects of the work in ensuring that questions related to the accuracy or integrity of any part of the work are appropriately investigated and resolved. The study was conducted in accordance with the Declaration of Helsinki (as revised in 2013). The study was approved by the medical ethics committee of National Cancer Center/National Clinical Research Center for Cancer/Cancer Hospital (NO. 20/250-2446) and individual consent for this retrospective analysis was waived. Animal experiments were performed under a project license (NO. NCC2020A292) granted by Animal Care and Use Committee of National Cancer Center/National Clinical Research Center for Cancer/Cancer Hospital, in compliance with institutional guidelines for the care and use of animals.

*Open Access Statement:* This is an Open Access article distributed in accordance with the Creative Commons Attribution-NonCommercial-NoDerivs 4.0 International License (CC BY-NC-ND 4.0), which permits the non-commercial replication and distribution of the article with the strict proviso that no changes or edits are made and the original work is properly cited (including links to both the formal publication through the relevant DOI and the license). See: <https://creativecommons.org/licenses/by-nc-nd/4.0/>.

## References

1. Gazdar AF, Bunn PA, Minna JD. Small cell lung cancer: what we know, what we need to know and the path forward. *Nat Rev Cancer* 2017;17:725-37.
2. Travis WD, Brambilla E, Nicholson AG, et al. The 2015 World Health Organization Classification of Lung Tumors: Impact of Genetic, Clinical and Radiologic Advances Since the 2004 Classification. *J Thorac Oncol* 2015;10:1243-60.
3. Jingjing Liu YC, Hui Li and Shuang Zhang. Current Status of Small Cell Lung Cancer in China. *Journal of Cancer Biology & Research* 2014;2:1032.
4. Torre LA, Siegel RL, Jemal A. Lung Cancer Statistics. *Adv Exp Med Biol* 2016;893:1-19.
5. Lewis DR, Check DP, Caporaso NE, et al. US lung cancer trends by histologic type. *Cancer* 2014;120:2883-92.
6. Park JY, Jang SH. Epidemiology of Lung Cancer in Korea: Recent Trends. *Tuberc Respir Dis (Seoul)* 2016;79:58-69.
7. Sabari JK, Lok BH, Laird JH, et al. Unravelling the biology of SCLC: implications for therapy. *Nat Rev Clin Oncol* 2017;14:549-61.
8. Rudin CM, Poirier JT. Small cell lung cancer in 2016: Shining light on novel targets and therapies. *Nat Rev Clin Oncol* 2017;14:75-6.
9. Nicholson AG, Chansky K, Crowley J, et al. The International Association for the Study of Lung Cancer Lung Cancer Staging Project: Proposals for the Revision of the Clinical and Pathologic Staging of Small Cell Lung Cancer in the Forthcoming Eighth Edition of the TNM Classification for Lung Cancer. *J Thorac Oncol* 2016;11:300-11.
10. Fukuoka M, Furuse K, Saijo N, et al. Randomized trial of cyclophosphamide, doxorubicin, and vincristine versus cisplatin and etoposide versus alternation of these regimens in small cell lung cancer. *J Natl Cancer Inst* 1991;83:855-61.
11. Rossi A, Di Maio M, Chiadini P, et al. Carboplatin- or cisplatin-based chemotherapy in first-line treatment of small cell lung cancer: the COCIS meta-analysis of individual patient data. *J Clin Oncol* 2012;30:1692-8.
12. van Niel G, D'Angelo G, Raposo G. Shedding light on the cell biology of extracellular vesicles. *Nat Rev Mol Cell Biol* 2018;19:213-28.
13. Becker A, Thakur BK, Weiss JM, et al. Extracellular Vesicles in Cancer: Cell-to-Cell Mediators of Metastasis. *Cancer Cell* 2016;30:836-48.
14. Wan M, Ning B, Spiegel S, et al. Tumor-derived exosomes (TDEs): How to avoid the sting in the tail. *Med Res Rev* 2020;40:385-412.
15. Syn N, Wang L, Sethi G, et al. Exosome-Mediated Metastasis: From Epithelial-Mesenchymal Transition to Escape from Immunosurveillance. *Trends Pharmacol Sci* 2016;37:606-17.
16. Mao S, Lu Z, Zheng S, et al. Exosomal miR-141 promotes tumor angiogenesis via KLF12 in small cell lung cancer. *J Exp Clin Cancer Res* 2020;39:193.
17. Syn NL, Wang L, Chow EK, et al. Exosomes in Cancer Nanomedicine and Immunotherapy: Prospects and Challenges. *Trends Biotechnol* 2017;35:665-76.
18. Fabian MR, Sonenberg N, Filipowicz W. Regulation of mRNA translation and stability by microRNAs. *Annu Rev Biochem* 2010;79:351-79.
19. Calin GA, Croce CM. MicroRNA signatures in human cancers. *Nat Rev Cancer* 2006;6:857-66.
20. He L, Zhu W, Chen Q, et al. Ovarian cancer cell-secreted

- exosomal miR-205 promotes metastasis by inducing angiogenesis. *Theranostics* 2019;9:8206-20.
21. Wang X, Luo G, Zhang K, et al. Hypoxic Tumor-Derived Exosomal miR-301a Mediates M2 Macrophage Polarization via PTEN/PI3Kgamma to Promote Pancreatic Cancer Metastasis. *Cancer Res* 2018;78:4586-98.
  22. Zhou Y, Ren H, Dai B, et al. Hepatocellular carcinoma-derived exosomal miRNA-21 contributes to tumor progression by converting hepatocyte stellate cells to cancer-associated fibroblasts. *J Exp Clin Cancer Res* 2018;37:324.
  23. Zhou W, Fong MY, Min Y, et al. Cancer-secreted miR-105 destroys vascular endothelial barriers to promote metastasis. *Cancer Cell* 2014;25:501-15.
  24. Zeng Z, Li Y, Pan Y, et al. Cancer-derived exosomal miR-25-3p promotes pre-metastatic niche formation by inducing vascular permeability and angiogenesis. *Nat Commun* 2018;9:5395.
  25. Fang JH, Zhang ZJ, Shang LR, et al. Hepatoma cell-secreted exosomal microRNA-103 increases vascular permeability and promotes metastasis by targeting junction proteins. *Hepatology* 2018;68:1459-75.
  26. Liu J, Han Y, Hu S, et al. Circulating Exosomal MiR-107 Restrains Tumorigenesis in Diffuse Large B-Cell Lymphoma by Targeting 14-3-3 $\eta$ . *Front Cell Dev Biol* 2021;9:667800.
  27. Abramovic I, Vrhovec B, Skara L, et al. MiR-182-5p and miR-375-3p Have Higher Performance Than PSA in Discriminating Prostate Cancer from Benign Prostate Hyperplasia. *Cancers (Basel)* 2021;13:2068.
  28. Benoist GE, van Oort IM, Boerrigter E, et al. Prognostic Value of Novel Liquid Biomarkers in Patients with Metastatic Castration-Resistant Prostate Cancer Treated with Enzalutamide: A Prospective Observational Study. *Clin Chem* 2020;66:842-51.
  29. Zhang Y, Zhang X, Situ B, et al. Rapid electrochemical biosensor for sensitive profiling of exosomal microRNA based on multifunctional DNA tetrahedron assisted catalytic hairpin assembly. *Biosens Bioelectron* 2021;183:113205.
  30. Fan K, Spassova I, Gravemeyer J, et al. Merkel cell carcinoma-derived exosome-shuttle miR-375 induces fibroblast polarization by inhibition of RBPJ and p53. *Oncogene* 2021;40:980-96.
  31. He Z, Li W, Zheng T, et al. Human umbilical cord mesenchymal stem cells-derived exosomes deliver microRNA-375 to downregulate ENAH and thus retard esophageal squamous cell carcinoma progression. *J Exp Clin Cancer Res* 2020;39:140.
  32. Dejana E. Endothelial cell-cell junctions: happy together. *Nat Rev Mol Cell Biol* 2004;5:261-70.
  33. Martin TA. The role of tight junctions in cancer metastasis. *Semin Cell Dev Biol* 2014;36:224-31.
  34. Yoda S, Soejima K, Hamamoto J, et al. Claudin-1 is a novel target of miR-375 in non-small cell lung cancer. *Lung Cancer* 2014;85:366-72.
  35. Poy MN, Eliasson L, Krutzfeldt J, et al. A pancreatic islet-specific microRNA regulates insulin secretion. *Nature* 2004;432:226-30.
  36. Yan JW, Lin JS, He XX. The emerging role of miR-375 in cancer. *Int J Cancer* 2014;135:1011-8.
  37. Mathe EA, Nguyen GH, Bowman ED, et al. MicroRNA expression in squamous cell carcinoma and adenocarcinoma of the esophagus: associations with survival. *Clin Cancer Res* 2009;15:6192-200.
  38. He XX, Chang Y, Meng FY, et al. MicroRNA-375 targets AEG-1 in hepatocellular carcinoma and suppresses liver cancer cell growth in vitro and in vivo. *Oncogene* 2012;31:3357-69.
  39. Ding L, Xu Y, Zhang W, et al. MiR-375 frequently downregulated in gastric cancer inhibits cell proliferation by targeting JAK2. *Cell Res* 2010;20:784-93.
  40. Hui AB, Bruce JP, Alajez NM, et al. Significance of dysregulated metadherin and microRNA-375 in head and neck cancer. *Clin Cancer Res* 2011;17:7539-50.
  41. Chang C, Shi H, Wang C, et al. Correlation of microRNA-375 downregulation with unfavorable clinical outcome of patients with glioma. *Neurosci Lett* 2012;531:204-8.
  42. Mazar J, DeBlasio D, Govindarajan SS, et al. Epigenetic regulation of microRNA-375 and its role in melanoma development in humans. *FEBS Lett* 2011;585:2467-76.
  43. de Souza Rocha Simonini P, Breiling A, Gupta N, et al. Epigenetically deregulated microRNA-375 is involved in a positive feedback loop with estrogen receptor alpha in breast cancer cells. *Cancer Res* 2010;70:9175-84.
  44. Wang Y, Lieberman R, Pan J, et al. miR-375 induces docetaxel resistance in prostate cancer by targeting SEC23A and YAP1. *Mol Cancer* 2016;15:70.
  45. Lu S, Kong H, Hou Y, et al. Two plasma microRNA panels for diagnosis and subtype discrimination of lung cancer. *Lung Cancer* 2018;123:44-51.
  46. Nishikawa E, Osada H, Okazaki Y, et al. miR-375 is activated by ASH1 and inhibits YAP1 in a lineage-dependent manner in lung cancer. *Cancer Res* 2011;71:6165-73.

47. Borromeo MD, Savage TK, Kollipara RK, et al. ASCL1 and NEUROD1 Reveal Heterogeneity in Pulmonary Neuroendocrine Tumors and Regulate Distinct Genetic Programs. *Cell Rep* 2016;16:1259-72.
48. Rudin CM, Poirier JT, Byers LA, et al. Molecular subtypes of small cell lung cancer: a synthesis of human and mouse model data. *Nat Rev Cancer* 2019;19:289-97.
49. Ruivo CF, Adem B, Silva M, et al. The Biology of Cancer Exosomes: Insights and New Perspectives. *Cancer Res* 2017;77:6480-8.
50. Rodrigues G, Hoshino A, Kenific CM, et al. Tumour exosomal CEMIP protein promotes cancer cell colonization in brain metastasis. *Nat Cell Biol* 2019;21:1403-12.
51. Wang D, Wang X, Si M, et al. Exosome-encapsulated miRNAs contribute to CXCL12/CXCR4-induced liver metastasis of colorectal cancer by enhancing M2 polarization of macrophages. *Cancer Lett* 2020;474:36-52.
52. Lin Y, Zhang C, Xiang P, et al. Exosomes derived from HeLa cells break down vascular integrity by triggering endoplasmic reticulum stress in endothelial cells. *J Extracell Vesicles* 2020;9:1722385.

**Cite this article as:** Mao S, Zheng S, Lu Z, Wang X, Wang Y, Zhang G, Xu H, Huang J, Lei Y, Liu C, Sun N, He J. Exosomal miR-375-3p breaks vascular barrier and promotes small cell lung cancer metastasis by targeting claudin-1. *Transl Lung Cancer Res* 2021;10(7):3155-3172. doi: 10.21037/tlcr-21-356

## Appendix: Supplementary methods

### *Small RNA sequencing*

A total of 2 ml of pooled plasma derived from five or six patients per sample was used to perform exosome isolation using ultracentrifugation. miRNeasy Mini Kit (QIAGEN) was used to isolate total RNA from plasma exosomes following the manufacturer's instruction. Isolated RNA was loaded on 1.5% agarose gels to evaluate its degradation and contamination followed by quantitative determination in the NanoDrop 2000 Spectrophotometer (Thermo Fisher Scientific). A total of 2.5 ng RNA per sample was used to construct small RNA library. RNA libraries were sequenced on the platform of Illumina HiSeq2500. Clean reads filtered for ribosomal RNA (rRNA), transfer RNA (tRNA), small nuclear RNA (snRNA), small nucleolar RNA (snoRNA), other noncoding RNA (ncRNA) and repeats were compared with the miRBase database to assess miRNA expression.

### *Exosome isolation and identification*

Exosomes were isolated from pooled plasma by ultracentrifugation for small RNA sequencing. Briefly, 2 ml of pooled plasma per sample was first centrifuged at 3,000  $\times$ g and 4 °C for 15 min to obtain supernatant followed by dilution with PBS. The diluted supernatant was then centrifuged at 13,000  $\times$ g and 4 °C for 30 min followed by filtration using a 0.22- $\mu$ m filter. The filtered sample was loaded into the ultracentrifuge and ultracentrifuged at 100,000  $\times$ g and 4 °C for 2 hours to collect exosomes. Exosome pellet was washed by resuspending it in PBS and was then ultracentrifuged at 100,000 g and 4 °C for 2 hours. Next, the obtained exosome pellet was dissolved in 100  $\mu$ L PBS for RNA extraction.

For exosomes isolation from plasma in cohort 2, the Total Exosome Isolation (from plasma) Kit (Invitrogen) was applied according to the instructions, and the expression of plasma exosomal miRNA was validated.

To isolate exosomes from the cell culture supernatant, fresh culture medium (CM) supplying with 10% exosome-depleted fetal bovine serum (FBS) was added to cells and collected 48 hours later. The CM was processed for centrifugation at 500  $\times$ g, 4 °C for 10 min, 2,000  $\times$ g, 4 °C for 10 min successively to remove cells and dead cells, subsequently passed through a 0.22- $\mu$ m Vacuum Filter System (Corning, cat. No. 431097) to remove large particles. The filtered supernatant was further concentrated by the Vivaflow 200 filtration system (Sartorius, cat. No.

VF20P4) and then ultracentrifuged at 110,000  $\times$ g and 4 °C for 70 min to precipitate exosomes. The exosome pellet was washed by dissolving it in PBS and ultracentrifuged once again, the final exosome sample was obtained by resuspending the second exosome precipitate in PBS and was stored at -80 °C for future use.

To characterize the isolated exosomes, transmission electron microscopy (JEOL-JEM1400, Tokyo, Japan) and ZetaView PMX 110 (Particle Metrix, Meerbusch, Germany) were used to capture the appearance and assess the diameter and number of exosomes, respectively. Western blotting was applied to identify exosome-related proteins, including CD9 and TSG101.

### *RNA isolation and qRT-PCR*

TRIzol-based (Invitrogen, USA) traditional method was performed to isolate total RNA from cells, exosomes or serum. Specifically, for the isolation of RNA from exosomes or serum, cel-miR-39 was spiked in before adding chloroform to serve as the external reference gene, 0.1 mg/mL glycogen (Invitrogen) was added in the process of isopropanol precipitation to make the RNA pellet visible.

For miRNA, TransScript Green miRNA Two-Step qRT-PCR SuperMix (TransGen Biotech, Beijing, China) was used for the qRT-PCR of miRNA with a universal primer and a specific forward primer. RNU6 served as the internal reference gene in cell-miRNA PCR, while cel-miR-39 served as the external reference gene in exosome- or serum-miRNA PCR. For mRNA, TransScript II All-in-One First-Strand cDNA Synthesis SuperMix for qPCR and TransStart Top Green qPCR SuperMix (TransGen Biotech, Beijing, China) were used for mRNA RT-PCR and qRT-PCR, respectively. GAPDH served as the internal reference gene in mRNA PCR. All qRT-PCRs were conducted on an ABI 7900HT RT-PCR thermocycler (Life Technologies).

### *Western blotting*

Proteins of exosomes or cells were harvested utilizing RIPA lysate buffer and protein concentrations were detected by the Bradford Protein Assay. Equivalent proteins from different samples were loaded for sodium dodecyl sulfate-polyacrylamide gel electrophoresis (SDS-PAGE). Separated proteins were then transferred to a polyvinylidene fluoride (PVDF) membrane followed by blocking with 5% milk for 1 hour at room temperature. After that, the diluted primary antibodies were added to incubate with the membranes

overnight at 4 °C. The next day, after incubation with HRP-conjugated secondary antibody for 1 hour at room temperature, the membranes were exposed and detected in an Amersham Imager 600. Antibodies used in this study were as follows: GAPDH (CST, #5174), claudin-11 (Abcam, ab175236), claudin-1 (CST, #13255), CD9 (Abcam, ab92726) and TSG101 (Abcam, ab83).

### ***Cell Immunofluorescence***

miR-375-3p mimic-transfected or exosome-treated HUVECs were plated on chamber slides (Biologix, Shandong, China) and cultured for 24–48 hours. Then, HUVECs were washed in PBS twice to remove dead cells and fixed in 4% paraformaldehyde solution for 10 min. After that, 0.2% Triton X-100/PBS was added to the chamber slides for 5 min to permeabilize the cell membranes. 5% BSA/PBS was used to block the non-specific binding sites of HUVECs and the primary antibodies (claudin-1, CST, #13995) were added to incubate overnight at 4 °C. The next day, after incubation with secondary antibody (CST, #4412) in the dark, the slides were covered by ProLong™ Gold Antifade Mountant with DAPI (Invitrogen) and then photographed under a confocal microscope.

### ***Liquid chromatography-mass spectrometry/mass spectrometry analysis (LC-MS/MS)***

Proteins extracted from miR-375- or NC-transfected HUVECs (each group had three replicates) were processed for LC-MS/MS in Applied Protein Technology (Shanghai, China). Protein samples were digested to collect peptides by the filter-aided proteome preparation (FASP) method. A total of 100 µg peptides of each sample was used for tandem mass tag (TMT, Thermo Fisher Scientific) labeling following the instruction. TMT-labeled peptides of each sample were mixed in equal amounts followed by fractionation into 10 fractions by the High pH Reversed-Phase Peptide Fractionation Kit (Thermo Fisher Scientific). Each fraction was loaded onto a reversed-phase trap column (Thermo Scientific Acclaim PepMap100, 100 µm × 2 cm, nanoViper C18) and separated by a C18-reversed-phase analytical column (Thermo Scientific Easy Column, 10 cm long, 75 µm inner diameter, 3 µm resin) at a flow rate of 300 nL/min. A Q Exactive mass spectrometer (Thermo Scientific) was used to conduct LC-MS/MS in a data-dependent top10 manner with a survey scan of 300–1,800 m/z. MS/MS spectra data were searched in Proteome Discoverer 1.4 software for protein identification and quantitative analysis.

**Table S1** The clinical and pathological characteristics of the pooled samples in cohort 1

		SCLC patients		Healthy volunteers	
		Sample 1	Sample 2	Sample 3	Sample 4
Sex	Female	4	2	4	2
	Male	1	4	1	4
Age	<60	2	6	3	6
	≥60	3	0	2	0
T	T1-T2	2	3	-	-
	T3-T4	3	3	-	-
N	N0-N1	0	0	-	-
	N2-N3	5	6	-	-
M	M0	0	6	-	-
	M1	5	0	-	-
Stage	III	0	6	-	-
	IV	5	0	-	-

SCLC, small-cell lung cancer.

**Table S2** The clinical and pathological characteristics of samples in cohort 2 and cohort 3

		Cohort 2 (82)		Cohort 3 (147)		
		SCLC (57)	Normal (25)	SCLC (69)	NSCLC (LUAD 20, LUSC 26)	Normal (32)
Sex	Female	22	13	14	18	10
	Male	35	12	55	28	22
Age	<60	29	22	28	25	14
	≥60	28	3	41	21	18
T	T1-T2	26	-	28	26	-
	T3-T4	31	-	41	20	-
N	N0-N1	19	-	10	12	-
	N2-N3	38	-	59	34	-
M	M0	45	-	40	29	-
	M1	12	-	29	17	-
Stage	I	9	-	4	1	-
	II	8	-	1	5	-
	III	28	-	35	23	-
	IV	12	-	29	17	-

SCLC, small-cell lung cancer; NSCLC, non-small-cell lung cancer; LUAD, lung adenocarcinoma; LUSC, lung squamous cell carcinoma.

**Table S3** Sequences of primers used for PCR

Gene	Forward primer	Reverse primer
miR-375	CTTTGTTTCGTTCCGGCTCGC	-
Cel-miR-39	TCACCGGGTGTAATCAGCTTG	-
RNU6	CTCGCTTCGGCAGCACA	-
Pri-miR-375	CGACGTGTCAGCCGCAGATG	CCTCGGTGATCTCCTGGTCCTG
Claudin-11	GGCTGGTGTTTTGCTCATTCTGC	AGCACCAATCCAGCCTGCATAC
Claudin-1	GTCTTTGACTCCTTGCTGAATCTG	CACCTCATCGTCTTCCAAGCAC
GAPDH	GTCTCCTCTGACTTCAACAGCG	ACCACCCTGTTGCTGTAGCCAA

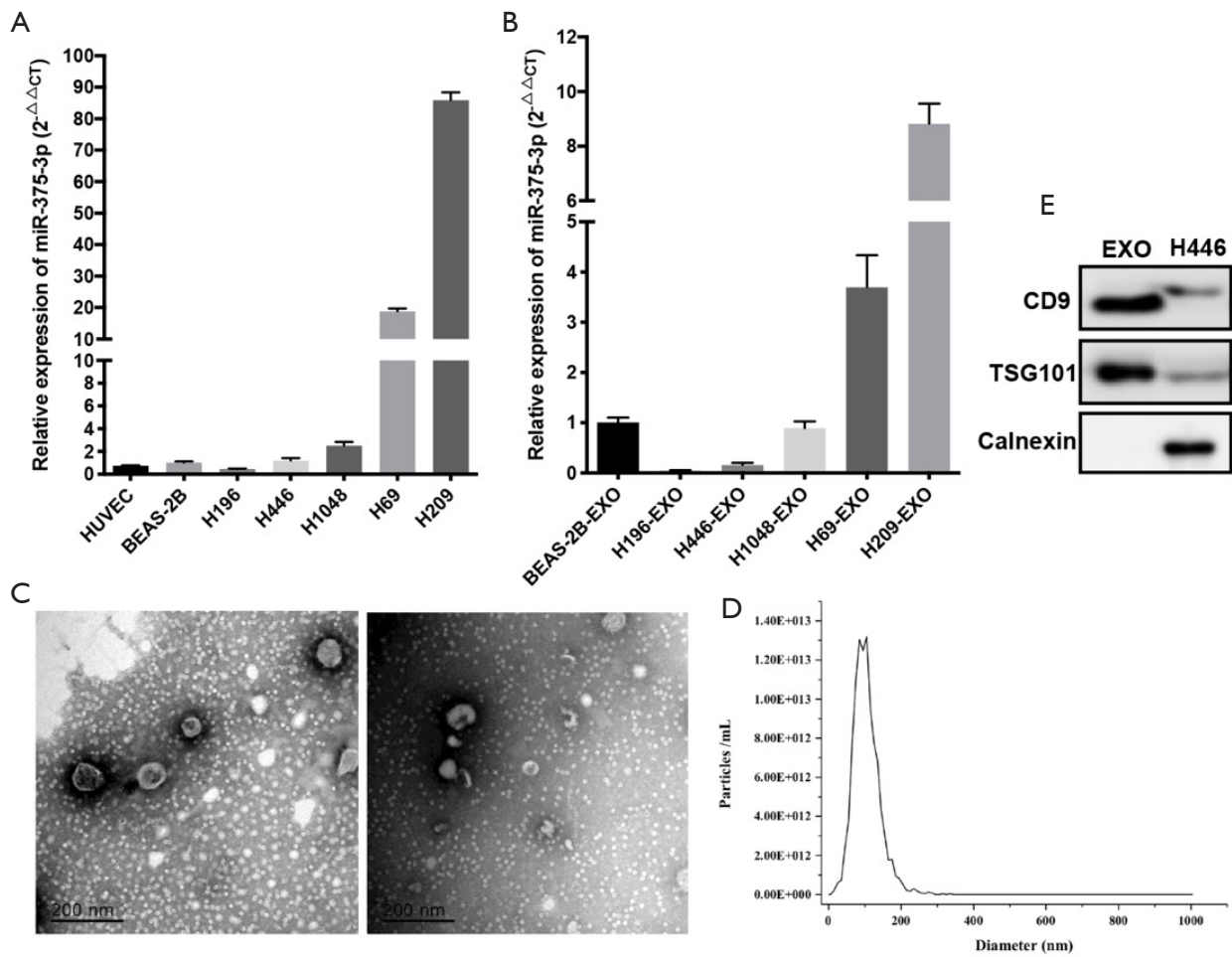


**Figure S1** H446 and H1048 cells and their exosomes had low endogenous levels of miR-375-3p. (A,B) The level of miR-375-3p in HUVECs, BEAS-2B cells and SCLC cells (A) and SCLC-cell-secreted exosomes (B). (C) Representative images of H446-cell-secreted exosomes under TEM. (D) Distribution of the particle size of H446-cell-secreted exosomes. (E) Western blot analysis of TSG101, CD9 and Calnexin in H446 cell-secreted exosomes and H446 cells. TEM, transmission electron microscopy.

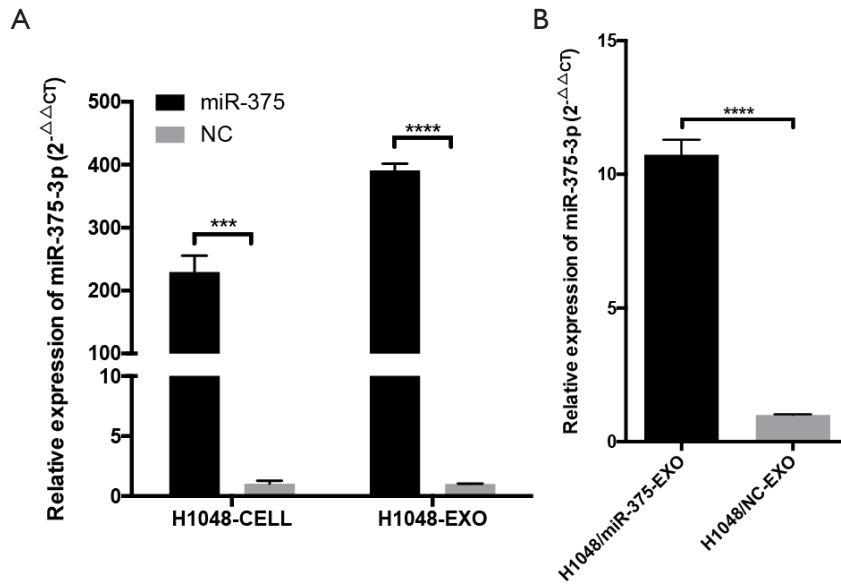


**Figure S2** H1048-cell-secreted exosomal miR-375-3p was absorbed by HUVECs. (A) The level of miR-375-3p in H1048 cells or H1048-cell-secreted exosomes after transfection with miR-375-3p mimics (miR-375) or negative control mimics (NC). (B) The level of miR-375-3p in HUVECs after incubation with H1048/miR-375-EXO or H1048/NC-EXO for 12 hours. H1048/miR-375-EXO, exosomes derived from miR-375-transfected H1048 cells; H1048/NC-EXO, exosomes derived from NC-transfected H1048 cells. \*\*\* $P < 0.001$ ; \*\*\*\* $P < 0.0001$ .

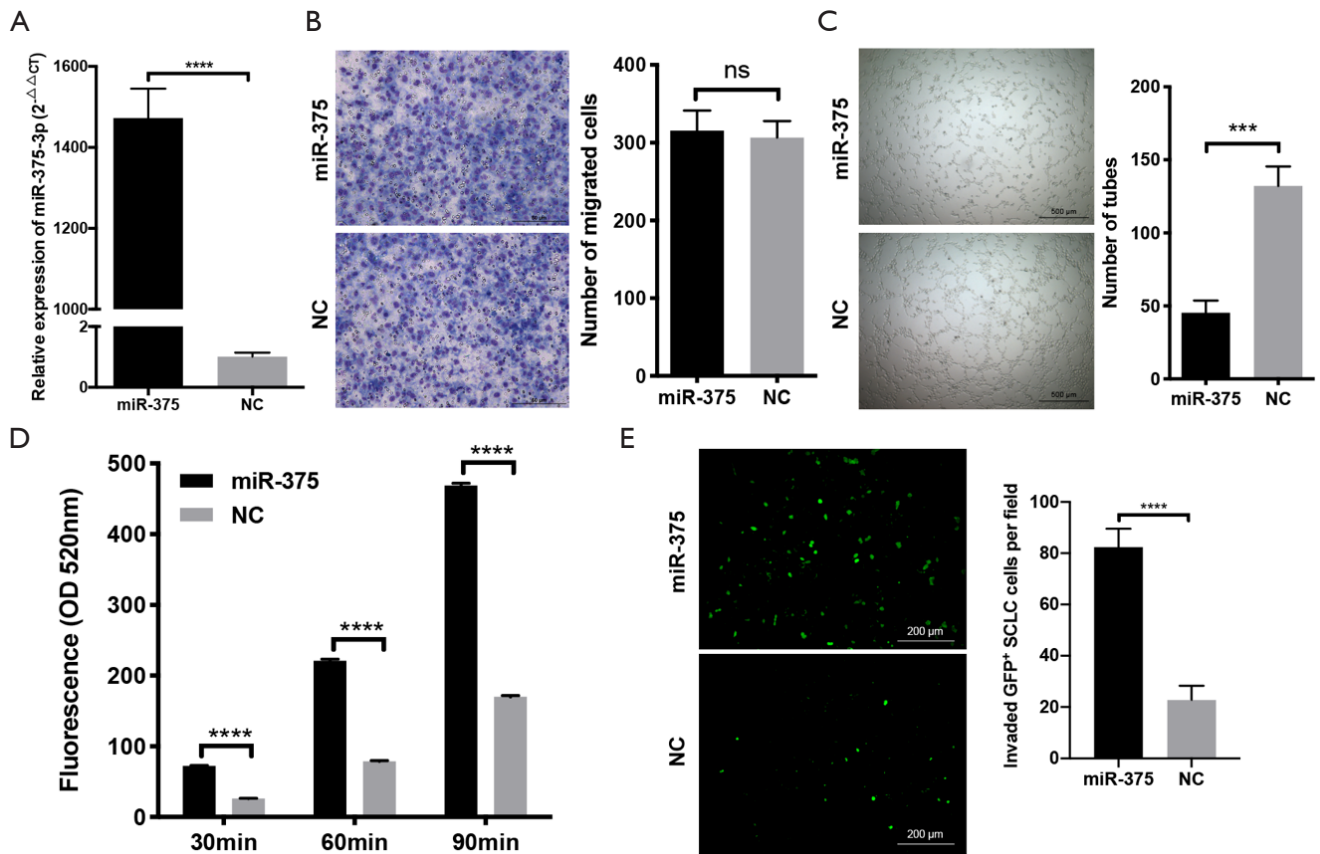


**Figure S3** Mimics of miR-375-3p induced the permeability of HUVEC monolayers. (A) The level of miR-375-3p in miR-375-3p mimics (miR-375) or negative control mimics (NC) transfected HUVECs. (B) Representative images of migrated HUVECs after transfection with miR-375 or NC, with the right bar chart indicating the number of migrated cells. (C) Representative images of tubes formed by HUVECs after transfection with miR-375 or NC, with the right bar chart indicating the number of formed tubes. (D) Fluorescence intensity of FITC-dextran passing through HUVEC monolayers after transfection with miR-375 or NC. (E) Representative images of GFP<sup>+</sup> SCLC cells migrated through miR-375- or NC-transfected HUVECs, with the right bar chart indicating the number of migrated cells. \*, P<0.001; \*\*, P<0.0001.

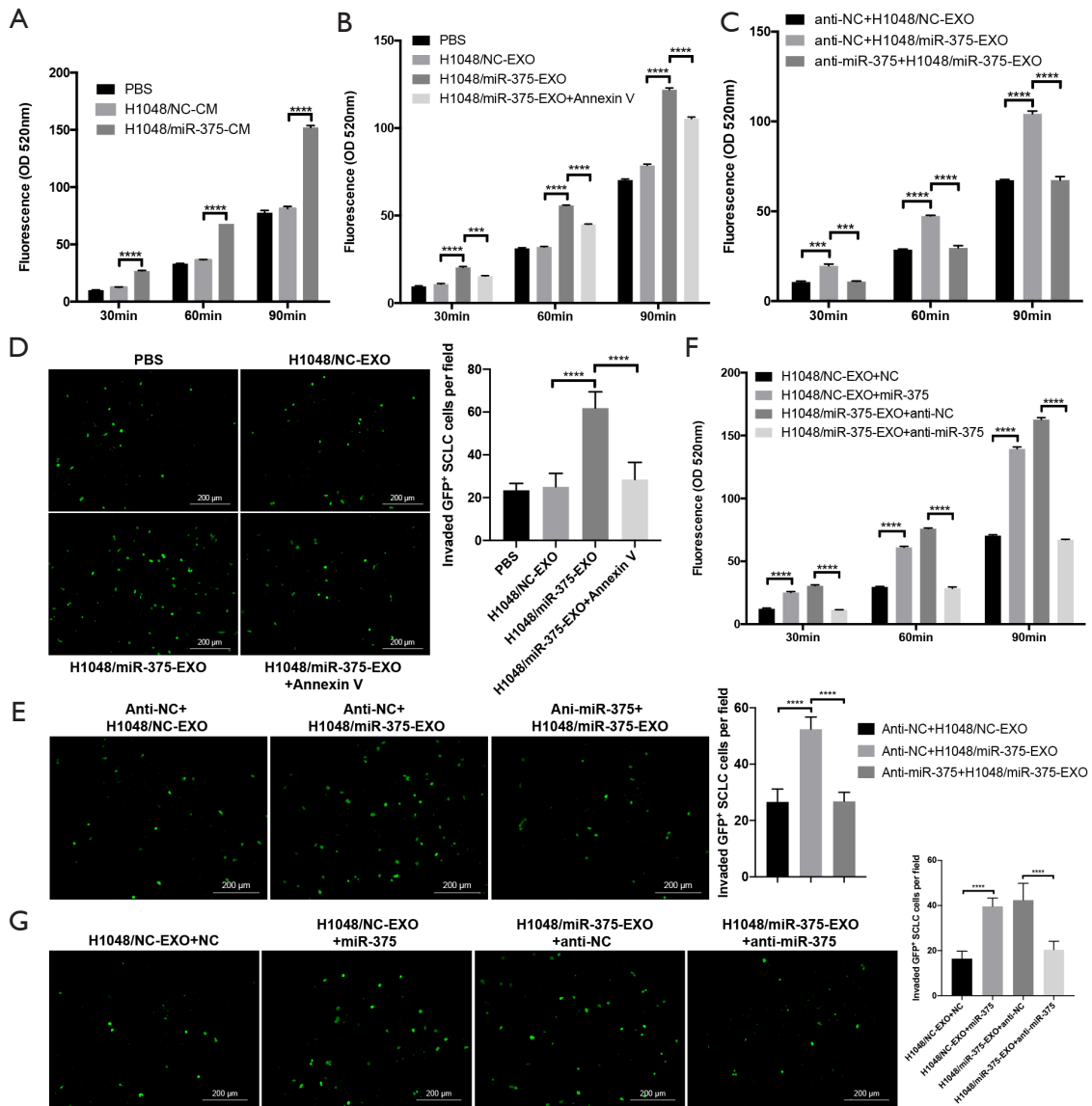


**Figure S4** Exosomal miR-375-3p secreted by H1048 cells induced the permeability of HUVECs and promoted SCLC cell transendothelial migration in vitro. (A) Fluorescence intensity of FITC-dextran passing through HUVEC monolayers treated with H1048/miR-375-CM or H1048/NC-CM. (B) Fluorescence intensity of FITC-dextran passing through HUVEC monolayers treated with H1048/miR-375-EXO, H1048/NC-EXO or Annexin V-blocked H1048/miR-375-EXO. (C) Fluorescence intensity of FITC-dextran passing through H1048/miR-375-EXO- or H1048/NC-EXO-treated HUVEC monolayers pre-transfected with anti-miR-375 or anti-NC. (D) Representative images of GFP+ SCLC cells migrated through H1048/miR-375-EXO- or H1048/NC-EXO-treated HUVEC monolayers, the right bar chart indicated the number of migrated cells. (E) Representative images of GFP+ SCLC cells migrated through H1048/miR-375-EXO- or H1048/NC-EXO-treated HUVEC monolayers pre-transfected with anti-miR-375 or anti-NC; the right bar chart indicated the number of migrated cells. (F) Fluorescence intensity of FITC-dextran passing through HUVEC monolayers treated with miR-375-3p-mimic-loaded H1048/NC-EXO or miR-375-3p-inhibitor-loaded H1048/miR-375-EXO. (G) Representative images of GFP+ SCLC cells that migrated through HUVEC monolayers treated with miR-375-3p-mimic-loaded H1048/NC-EXO or miR-375-3p-inhibitor-loaded H1048/miR-375-EXO, the right bar chart indicated the number of migrated cells. H1048/miR-375-CM, culture medium derived from miR-375-transfected H1048 cells; H1048/NC-CM, culture medium derived from NC-transfected H1048 cells; H1048/miR-375-EXO, exosomes derived from miR-375-transfected H1048 cells; H1048/NC-EXO, exosomes derived from NC-transfected H1048 cells; anti-miR-375, miR-375-3p inhibitors; anti-NC, negative control inhibitors; \*\*\* $P < 0.001$ ; \*\*\*\* $P < 0.0001$ .

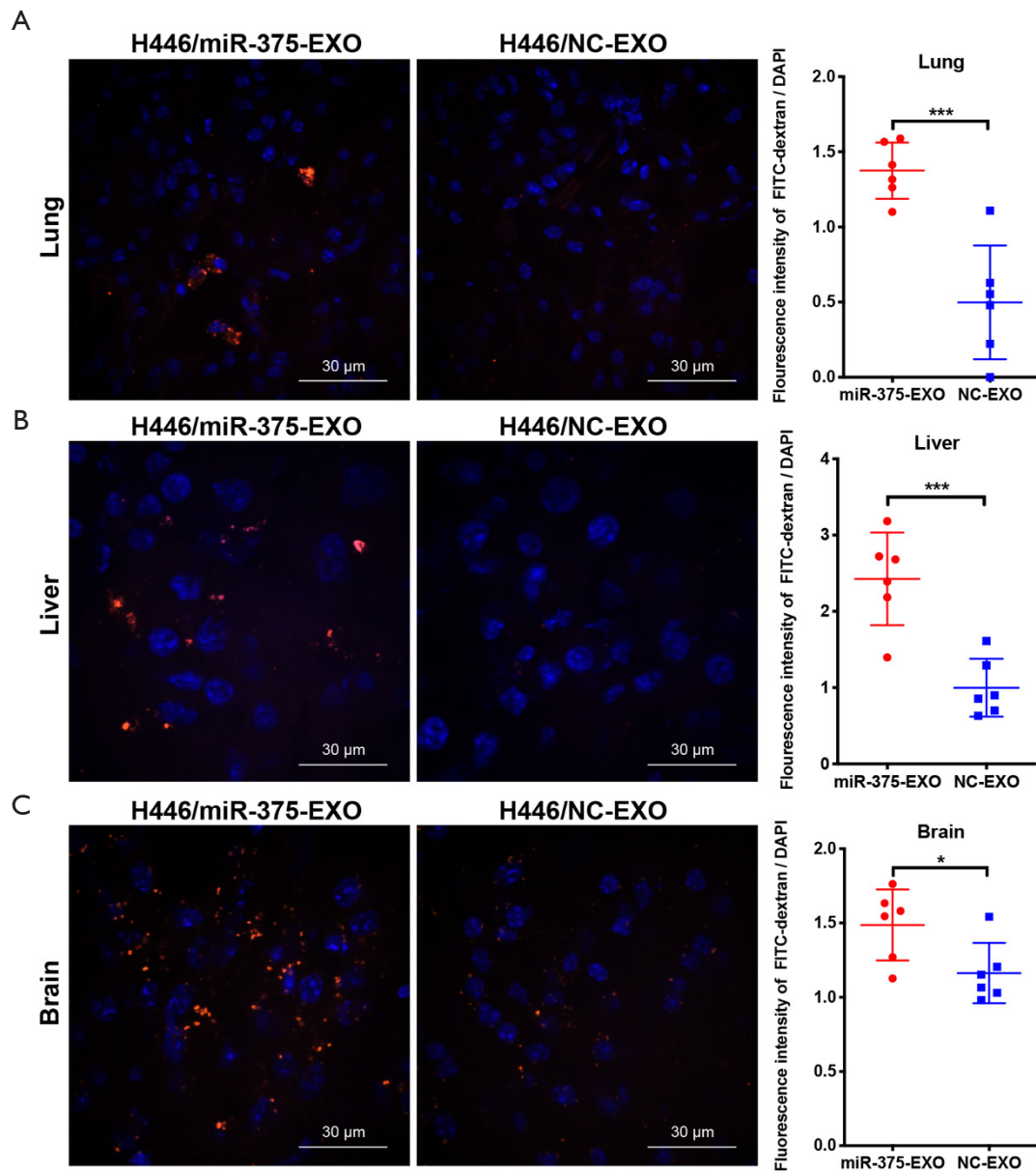


**Figure S5** H446-cell-derived exosomal miR-375-3p induced the permeability of blood vessels *in vivo*. (A-C) Representative images of infiltrated FITC-dextran in the lung (A), liver (B) and brain (C) tissues of mice after treatment with H446/miR-375-EXO or H446/NC-EXO, with the red fluorescence indicating the infiltrated FITC-dextran, the blue fluorescence indicating the nucleus of cells and the right bar chart indicating the relative fluorescence intensity. H446/miR-375-EXO, exosomes derived from miR-375-transfected H446 cells; H446/NC-EXO, exosomes derived from NC-transfected H446 cells. \* $P < 0.05$ ; \*\*\* $P < 0.001$ .

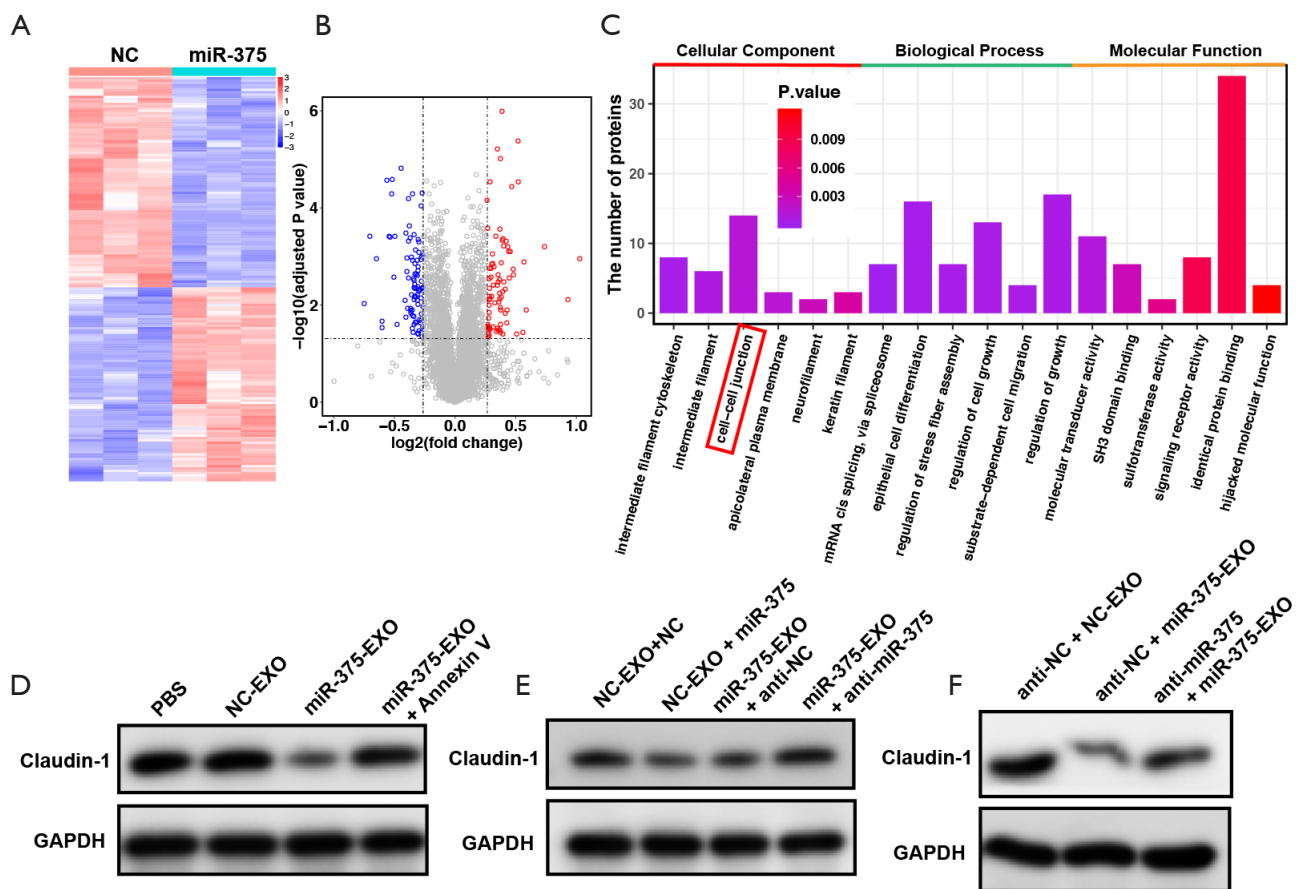


**Figure S6** miR-375-3p inhibited the expression of tight junction protein claudin-1. (A,B) Heatmap (A) and volcano plot (B) of dysregulated proteins discovered by protein mass spectrometry analysis in miR-375-3p mimics (miR-375) or negative control mimics (NC) transfected HUVECs. (C) GO enrichment analysis in the dysregulated proteins discovered by protein mass spectrometry analysis. (D) Western blot analysis of claudin-1 in HUVECs that were incubated with PBS, NC-EXO, miR-375-EXO or Annexin V-pretreated miR-375-EXO. (E) Western blot analysis of claudin-1 in HUVECs after incubation with miR-375-3p-mimic-loaded NC-EXO (NC-EXO + miR-375) and its negative control (NC-EXO + NC), miR-375-3p-inhibitor-loaded miR-375-EXO (miR-375-EXO + anti-miR-375) and its negative control (miR-375-EXO + anti-NC). (F) Western blot analysis of claudin-1 in NC-EXO- or miR-375-EXO-treated HUVECs that were pre-transfected with anti-miR-375 or anti-NC.

Table S4 Differentially expressed proteins identified by mass spectrometry analysis

Gene Name	Coverage	Unique Peptides	Peptides	PSMs	AAs	MW [kDa]	calc. pI	Group1-1/REF	Group1-2/REF	Group1-3/REF	average Group1	Group2-1/REF	Group2-2/REF	Group2-3/REF	average Group2	Group1/Group2	t test p value
MGAT4B	3.28	1	1	1	548	63.1587689	7.86962891	1.272983368	1.309962404	1.460677808	1.347874527	0.583875897	0.777477507	0.625299812	0.662217739	2.833395	0.00113
SDC1	5.48	1	1	2	310	32.441856	4.62744141	1.233001664	1.511600299	1.118344105	1.287648689	0.602955052	0.687027066	0.735941126	0.673307718	1.500758	0.007618
WBP4	2.66	1	1	1	376	42.4809435	5.56688453	1.185473155	1.255214954	1.826516799	0.826166152	0.730630704	0.753543587	1.665758	0.00603		
NOLC1	24.46	21	21	40	699	73.5596396	9.46630859	1.36027985	1.039897395	1.204399253	1.2015255	0.812381554	0.806048562	0.783417857	0.800615991	1.502751	0.012498
H6XIM1	1.98	5	5	7	359	40.5984789	4.89404297	1.247062522	1.150649436	1.158272192	1.18532890	0.857620137	0.809779711	0.733281192	0.800227013	1.48124	0.001272
ADAM15	11.87	5	1	1	863	92.891969	6.72705806	1.096115388	1.116268046	1.376712755	1.196365394	0.81564258	0.957579999	0.666304825	0.813210761	1.471163	0.036109
TOR4A	6.86	3	3	4	423	46.849381	9.93505859	1.1893961	1.167909729	1.186556092	1.181315144	0.792916805	0.840809965	0.837899973	0.823632915	1.434274	2.86E-05
SETD7	2.19	1	1	1	366	40.6951182	4.62744141	1.172002531	1.197378307	1.174709515	1.181483455	0.818605523	0.836253229	0.821301422	0.826177468	1.43096	4.21E-06
PAN3	1.13	1	1	1	887	95.5521789	8.57275391	1.339954094	1.019718105	1.173432901	1.177071715	0.963606332	0.787562275	0.734474348	0.828647648	1.421405	0.039072
MFN1	1.75	1	1	1	741	84.1061655	6.32861328	1.08623232	1.171449845	1.250161077	1.169279747	0.838614455	0.85492205	0.821784519	0.838440341	1.384588	0.002376
ZCCHC3	2.23	1	1	1	403	43.5199085	8.52808059	1.204852932	1.19734775	1.103878466	1.166969314	0.813733321	0.901336781	0.803456479	0.83950086	1.382116	0.001848
OGFR	19.65	11	11	12	677	73.2801494	4.84326172	1.162310731	1.128654549	1.161281075	1.157415452	0.840269693	0.833081093	0.843118625	0.838823137	1.379809	3.65E-05
IFT27	4.84	1	1	1	186	20.4673311	5.41455078	1.159707317	1.208919791	1.113743522	1.16079021	0.80782926	0.878544838	0.854089007	0.848672257	1.370373	0.00078
BCL2L1	3.86	1	1	1	233	26.0327034	4.9212891	1.164658132	1.192489718	1.111394399	1.152624903	0.894045519	0.77048493	0.886298027	0.850276159	1.358904	0.00271
SDC4	11.11	2	2	3	198	21.6280324	4.50048828	1.088607336	1.199984124	1.161109771	1.14990041	0.83690875	0.854387064	0.849663061	0.846716292	1.35897	0.000788
CCDC9	4.14	3	3	3	531	59.670617	5.40185547	1.217018667	1.128013926	1.149535149	1.164856014	0.870535925	0.883397734	0.830252985	0.861395548	1.352989	0.000628
SLFN11	5.44	3	4	4	901	52.769552	7.76708984	1.201798579	1.12904321	1.144650743	1.158526466	0.882034827	0.844107218	0.758176066	0.86143937	1.344873	0.012502
CANT1	6.23	2	2	3	401	44.8180909	6.08740234	1.099990236	1.133255189	1.18740305	1.14039991	0.823080005	0.928589651	0.695603463	0.844909807	1.343134	0.022847
G3BP2	29.67	9	11	23	482	54.0878091	5.55419222	1.144662578	1.157658588	1.128591858	1.143739941	0.897324563	0.897324563	0.80601763	0.854366591	1.335889	0.000482
MRPL54	7.25	1	1	3	138	15.8091817	9.59814453	1.093297885	1.107362117	1.248178635	1.149612879	0.846398457	0.880670376	0.864068802	0.863712545	1.331013	0.004775
CDK14	2.99	1	2	2	469	53.0233239	8.92431641	1.092577067	1.142672333	1.2021893	1.1458129	0.762326392	0.875420293	0.849515417	0.861804613	1.329551	0.014655
TRAPP5C	6.31	1	1	1	188	20.7071504	9.65673828	1.216492209	1.099841341	1.108810597	1.141748049	0.859123662	0.939792029	0.907112683	0.863610201	1.322084	0.003327
CXorf56	4.95	1	1	1	222	25.6079978	8.73388672	1.17096341	1.145661981	1.106450944	1.141025445	0.877317213	0.895777275	0.826413759	0.866502749	1.310817	0.006004
MESD	21.79	3	3	4	234	26.063057	7.78173828	1.123007063	1.124732806	1.173787489	1.140509119	0.878411977	0.893237603	0.829113152	0.86692091	1.315588	0.000431
CWC25	2.82	3	1	1	425	49.6169925	10.18402	1.274379263	1.090182834	1.052126204	1.1388991	0.884630726	0.816766026	0.802500911	0.867766015	1.312448	0.003936
CEP152	0.47	1	1	3	1710	195.504004	5.60498047	1.064707998	1.153737489	1.197221137	1.138555541	0.810726018	0.885967587	0.90758189	0.868091832	1.311561	0.005187
DENR	32.32	6	6	9	198	22.0780714	5.3002927	1.17791874	1.092139115	1.139548606	1.136535167	0.881055136	0.865471024	0.861011077	0.869179139	1.307296	0.000471
HABP4	4.12	2	2	3	413	43.7575684	5.4947266	1.129604209	1.119808367	1.13292114	1.125931239	0.858609555	0.859655	0.869455761	0.862571872	1.303919	1.01E-06
TPM4	57.66	7	23	77	248	26.5044925	4.69091797	1.064053497	1.160141718	1.15000218	1.124732465	0.850230504	0.854898583	0.887992183	0.864402847	1.301167	0.00135
KIAA1671	1.72	2	2	2	1806	196.590225	8.47201184	1.179035124	1.100366641	1.111374993	1.130264919	0.850439634	0.804942986	0.804942986	0.807039412	1.305996	0.006761
GALM	4.09	1	1	1	342	37.7421329	6.63808059	1.224781919	1.024204325	1.15118949	1.133391911	0.954285298	0.867324468	0.797201843	0.87293987	1.298362	0.0246
KDM2A	2.07	2	2	3	912	32.707543	7.57660619	1.161798579	1.115926219	1.109008667	1.128799955	0.764287926	0.884182563	0.963104224	0.870524904	1.298889	0.012688
PFN2	27.14	4	4	4	140	15.0362664	6.99072266	1.1152044	1.117277908	1.129590616	1.129590616	0.851337506	0.878419935	0.865847297	1.294328	9.54E-06	
EPHA8	2.09	1	2	2	1005	110.931575	8.00005859	1.034937446	1.119679001	1.239585583	1.131400677	0.762303476	0.89072336	0.961277243	0.874217685	1.294196	0.036977
RRBP1	62.06	76	78	175	1410	152.364688	8.60205708	1.191953892	1.125759936	1.166746135	1.128753321	0.837753873	0.925316341	0.855954549	0.873008254	1.293847	0.011374
SULT1B1	7.09	1	1	1	296	34.87664	7.06396484	1.139920454	1.127261736	1.130472398	1.132550829	0.906685148	0.966529031	0.727211619	0.876080599	1.291674	0.032076
CEP131	12.37	12	12	12	1083	122.075144	5.68904111	1.166106608	1.100687279	1.110342639	1.125711716	0.862542596	0.817876543	0.872291721	1.290523	0.000257	
SLC4A1AP	9.8	5	5	5	796	88.7590173	8.18683516	1.180849881	1.066192234	1.136440518	1.127815756	0.86513448	0.847707026	0.875286833	1.29851	0.002928	
CNTRL	0.77	1	3	4	2325	268.71966	5.55419922	1.204583265	1.066065457	1.117893797	1.129514173	0.903014881	0.897913782	0.830152536	0.877027066	1.28789	0.005683
TIMELESS	4.84	5	5	5	1208	138.571756	5.40185547	1.187566207	1.033708105	1.105418127	1.10889748	0.882647325	0.882748413	0.819565766	0.861863805	1.288958	0.007343
PPP1R18	13.67	5	5	10	613	67.9015087	5.40185547	1.052029004	1.166506212	1.166685803	1.128407006	0.827764633	0.812867202	0.899629824	0.890118663	1.282108	0.008513
PAFAH1B2	13.54	2	2	3	229	25.5531238	5.92238328	1.117471573	1.179064222	1.081386953	1.125974249	0.983214293	0.743767304	0.913839372	0.890273656	1.279118	0.032708
NSMCE2	4.45	1	1	1	247	27.914992	7.73739297	1.057768911	1.142488272	1.176302449	1.125519877	0.887564445	0.885173159	0.872202677	0.88167467	1.278611	0.003371
SIRT2	1.8	1	1	1	389	43.1544412	5.36378953	1.107211811	1.102293216	1.164730696	1.102723916	0.845745513	0.86642528	0.88172037	1.273602	0.002776	
GOLGA2	17.17	13	13	13	1002	113.016648	5.02099609	1.123220111	1.10520855	1.116660428	1.114730329	0.8416494	0.86481697	0.878361029	0.875804402	1.272808	6.15E-06
TBC1D10B	4.83	4	4	4	808	87.1447384	9.19789828	1.15968088	1.064196857	1.134750565	1.113542754	0.852300039	0.915450947	0.87511029	0.875011502	1.272604	0.003956
ISCA1	24.03	2	2	3	129	14.1704382	9.07800078	1.248113106	1.036286924	1.10706886	1.13048963	0.920722519	0.935446556	0.811477931	0.889215668	1.271933	0.030451
BCAS3	1.51	1	1	1	928	101.172123	6.69775391	1.080260551	1.053111733	1.222946732	1.120696332	0.829396019	0.950747488	0.78038513	0.882702879	1.263438	0.035276
GDI1	53.02	11	18	48	447	50.5501449	5.13525391	1.092122102	1.143559179	1.10857959	1.114750994	0.855963156	0.891907859	0.903466435	0.88377915	1.261346	0.000771
ERO1A	26.07	12	12	21	468	54.3580549	5.68115234	1.040127592	1.174377194	1.133216307	1.115907031	0.869741578	0.860632612	0.941772324	0.890715505	1.252021	0.008886
IRAK2	3.52	2	2	3	625	69.3888199	5.71923828	1.108944392	1.118013208	1.113627562	1.113528527	0.899220127	0.9399653	0.840341276	0.893169568	1.240716	0.001617
WBP11	24.02	16	16	24	641	69.9539239	3.88232422	1.164914904	1.041655472	1.110145064	1.10571814	0.89772188	0.876589731	0.88902747	0.887779694	1.245322	0.003836
SPATA20	1.27	1	1	1	786	87.8413143	7.43019758	1.227176508	1.081922034	1.023855581	1.110984708	0.88					

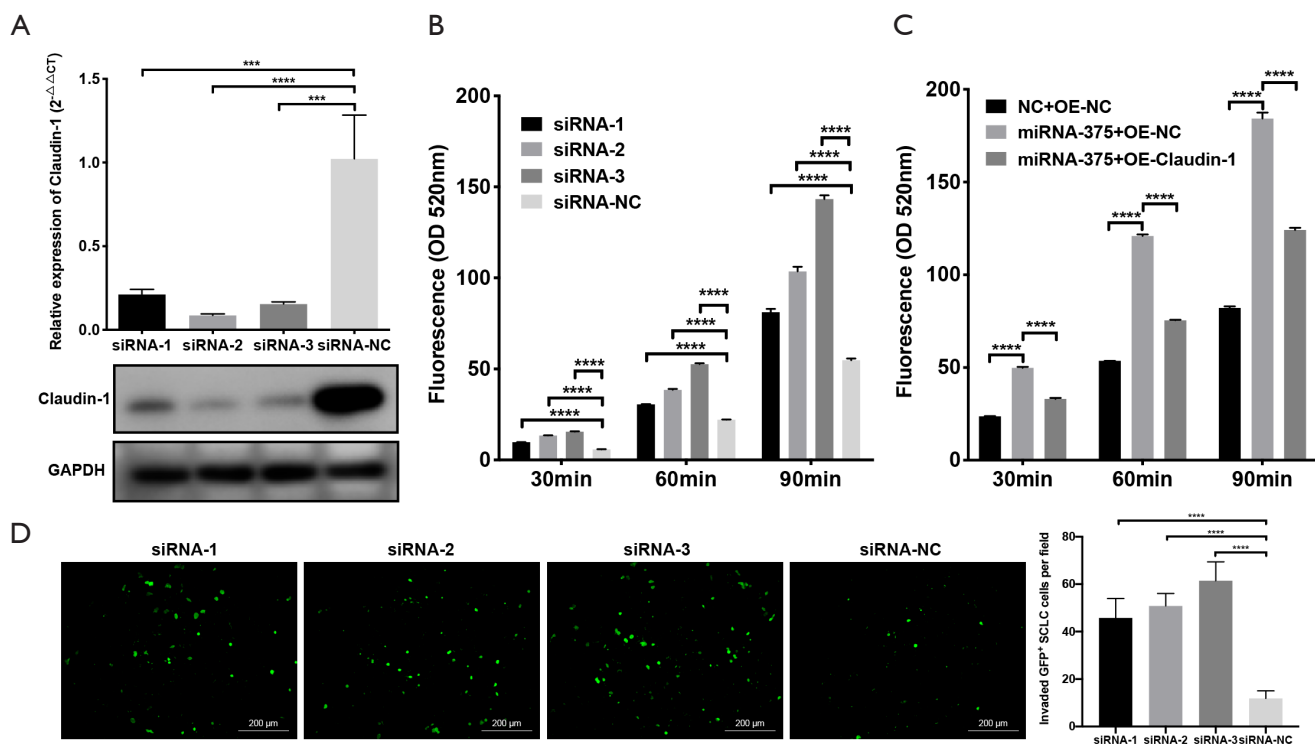


**Figure S7** Knocking down the expression of claudin-1 increased the permeability of HUVECs monolayers. (A) Both the RNA and protein expression of claudin-1 in HUVECs were downregulated by three claudin-1-specific siRNAs. (B) The downregulation of claudin-1 in HUVECs induced the permeability of HUVEC monolayers. (C) The increased permeability of HUVEC monolayers induced by miR-375-3p was abrogated by the upregulation of claudin-1. (D) The downregulation of claudin-1 in HUVECs promoted the transendothelial migration of GFP + SCLC cells. \*,  $P < 0.001$ ; \*\*,  $P < 0.0001$ .